Arabian Journal of Chemistry (2023) **16**, 104612

King Saud University

Arabian Journal of Chemistry

www.ksu.edu.sa
www.sciencedirect.com

ORIGINAL ARTICLE

Design, synthesis, docking and mechanistic studies of new thiazolyl/thiazolidinylpyrimidine-2,4-dione antiproliferative agents

Ashraf A. Aly [a,*], Mohammed B. Alshammari [b], Akil Ahmad [b], Hesham A. M. Gomaa [c], Bahaa G. M. Youssif [d,*], Stefan Bräse [e,f,*], Mahmoud A. A. Ibrahim [g], Asmaa H. Mohamed [a]

[a] *Chemistry Department, Faculty of Science, Minia University, 61519 El-Minia, Egypt*
[b] *Chemistry Department, College of Sciences and Humanities, Prince Sattam Bin Abdulaziz University, Al-Kharij, Saudi Arabia*
[c] *Department of Pharmacology, College of Pharmacy, Jouf University, Sakaka 72341, Aljouf, Saudi Arabia*
[d] *Pharmaceutical Organic Chemistry Department, Faculty of Pharmacy, Assiut University, 71526 Assiut, Egypt*
[e] *Institute of Organic Chemistry, Karlsruher Institut fur Technologie, 76131 Karlsruhe, Germany*
[f] *Institute of Biological and Chemical Systems (IBCS-FMS), Karlsruhe Institute of Technology, 76344 Eggenstein Leopoldshafen, Germany*
[g] *Computational Chemistry Laboratory, Chemistry Department, Faculty of Science, Minia University, Minia 61519, Egypt*

Received 20 November 2022; accepted 18 January 2023
Available online 24 January 2023

KEYWORDS

Uracil;
Thiazoles;
Thiazolidines;
Antiproliferative;
Kinases;
Docking

Abstract In this article, we display on the synthesis and biological evaluation of a new series of thiazolylpyrimidine **3a-l** and thiazolidinylpyrimidine derivatives **5a-e**. The structures of the new compounds were confirmed by using different spectral techniques including NMR, IR, mass spectroscopy in addition to elemental analyses. The cell viability of the new compounds was assessed against normal human mammary gland epithelial (MCF-10A) cell line. Data revealed that none of the compounds examined exhibited cytotoxic effects, and the cell viability for the compounds examined at 50 μM was greater than 87%. The antiproliferative activity of **3a-l** and **5a-e** was evaluated against four human cancer cell lines where the compounds showed promising activity. The most potent derivatives were compounds **3a**, **3c**, **3f**, **3i**, and **5b** with GI_{50} values ranging from

* Corresponding authors at: Chemistry Department, Faculty of Science, Minia University, 61519, El-Minia, Egypt(A.A. Aly), Institute of Organic Chemistry, Karlsruher Institut fur Technologie, 76131 Karlsruhe, Germany(S. Bräse), Pharmaceutical Organic Chemistry Department, Faculty of Pharmacy, Assiut University, Assiut 71526, Egypt(B.G.M. Youssif).
E-mail addresses: ashraf.shehata@mu.edu.eg, stefan.braese@kit.edu (A.A. Aly), bgyoussif@ju.edu.sa (B. G. M. Youssif), ashraf.shehata@mu.edu.eg, stefan.braese@kit.edu (S. Bräse).
Peer review under responsibility of King Saud University.

Production and hosting by Elsevier

https://doi.org/10.1016/j.arabjc.2023.104612

0.90 μM to 1.70 μM against the four cancer cell lines in comparison to doxorubicin (GI_{50} = 1.10 μM). Compounds **3a**, **3c** and **3i** showed potent antiproliferative activity with dual inhibitory action against EGFR and $BRAF^{V600E}$. Compounds **3a**, **3c**, and **3i** demonstrated promising AutoDock scores towards EGFR and $BRAF^{V600E}$ with values of − 9.1 and − 8.6, −9.0 and − 8.5, and − 8.4 and − 8.0 kcal/mol, respectively. The physicochemical and pharmacokinetic characteristics of **3a**, **3c**, and **3i** were anticipated, demonstrating their oral bioavailability.

1. Introduction

In anti-cancer research, a better understanding of druggable targets influences the development of new drugs. This strategy assumes that altering a specific cancer biomarker will result in a successful therapeutic outcome (Stanković et al., 2019). Selective anti-cancer drugs should be more effective at eliminating tumors while minimizing side effects on normal cells (Raghavendra et al., 2018). However, due to medication resistance, inhibiting just one target frequently has only a transient effect (Fu et al., 2017). Given the diversity of cancers, simultaneous intervention on multiple targets is required to achieve the best results (Zha et al., 2017). Combination chemotherapy is one method for simultaneously inhibiting two or more targets. However, differences in the pharmacokinetic profiles and metabolic stabilities of two or more medications are common.

Furthermore, combined chemotherapy may result in risky medication interactions (Palmeira et al., 2012). These problems could be solved by combining two medications with a single molecule that acts on several relevant targets (Zheng et al., 2017). In recent years, there has been much interest in multi-target medicines, also known as "hybrid" compounds, which have been developed by joining two or more separate pharmacophore moieties into a single molecule either directly through a covalent bond or indirectly through a linker (Mahboobi et al., 2010). Multi-target anti-cancer drugs have a wider range of activity than conventional medicines because they combine two different pharmacological features and target multiple signaling pathways (Alam et al., 2019, 2018; Banerji et al., 2018; Beckers et al., 2012; Cai et al., 2010).

The acquired $BRAF^{V600E}$ mutation was suggested as a resistance mechanism following therapy with EGFR inhibitors (Ho et al., 2017). The feedback activation of EGFR signaling is also linked to the emergence of resistance in colorectal cancer (Hyman et al., 2015). Furthermore, BRAF inhibition may result in EGFR activation, which fuels tumor growth (Desai et al., 2017). To treat these issues, BRAF/EGFR were used in tandem. Several studies have shown that the BRAF-EGFR combination has a significant therapeutic effect in people with metastatic colorectal cancer who have the $BRAF^{V600E}$ mutation (Ho et al., 2017). As a result, inhibiting the two kinases sequentially may address the issue of EGFR activation.

The pyrimidine ring is a popular heterocyclic scaffold in medicinal chemistry. Pyrimidine derivatives are widely used in medicine because of their therapeutic benefits (Bai et al., 2018; Borik et al., 2018; Jin et al., 2018; Madhu Sekhar et al., 2018; Rizk et al., 2018; Saleeb et al., 2018). The pyrimidine ring is also a component of DNA nucleic acid. Various drugs containing the pyrimidine nucleus are being used as effective anti-cancer agents via various mechanisms of action, i.e., 5-Fluorouracil (5-FU) **I** as thymidylate synthase inhibitor (Santi et al., 1974), Merbarone **II** as DNA topoisomerase II (topo II) inhibitor (Pastor et al., 2012), Nilotinib **III** and Imatinib **IV** as tyrosine kinase inhibitors (El-Mezayen et al., 2017; Shaker et al., 2013), and Ibrutinib (IBR) **V** as Bruton's tyrosine kinase (BTK) inhibitor (Tang et al., 2018) (Fig. 1).

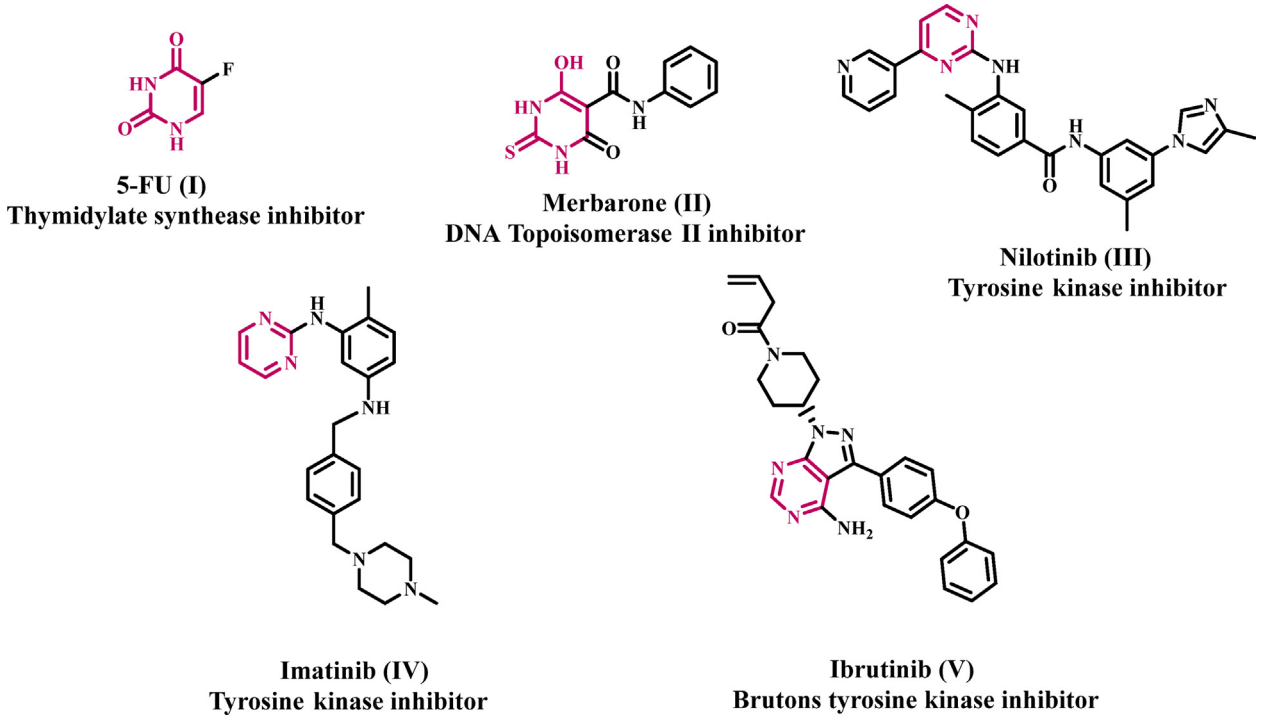

Fig. 1 Some selected pyrimidine-based anti-cancer drugs **I-V.**

On the other hand, thiazole, a five-membered heterocyclic ligand containing sulfur and nitrogen, has recently piqued the interest of researchers due to its potent biological properties (Ayati et al., 2015; Sharma et al., 2017).

Thiazole and its derivatives are among the most active compounds with a wide range of activity, with anti-cancer activity topping the list (Lozynskyi Andrii et al., 2014). Furthermore, thiazole-containing compounds have been found in several clinically available anti-cancer drugs (Fig. 2), including tiazofurin **(VI)** (IMP dehydrogenase inhibitor) (Franchetti et al., 1995), dasatinib **(VII)** (Bcr-Abl tyrosine kinase inhibitor) (Li et al., 2009), and dabrafenib **(VIII)** (B-RAF inhibitor) (Hu-Lieskovan et al., 2015).

Lv et al. developed two thiazolidinone derivatives to inhibit EGFR and HER-2 kinases. Some of the synthesized compounds exhibited significant EGFR and HER-2 inhibitory activity. Compound **(IX)** demonstrated the most potent EGFR and HER-2 inhibitory activities with IC_{50} values of 0.09 μM and 0.42 μM, respectively,e that some of the thiazolidinone derivatives have Fig. 2 (Lv et al., 2010). In another study, Zhao et al. prepared a series of thiazole-based derivatives and evaluated them as potential inhibitors of $BRAF^{V600E}$. According to the biological activity data, compound **(X,** Fig. 2**)** exhibited the most potent antiproliferative activity with potent $BRAF^{V600E}$ inhibitory activity with an IC_{50} value of 0.05 μM. Furthermore, compound **X** induced remarkable apoptosis dose-dependent (Abdel-Maksoud et al., 2015).

Motivated by the findings above and as an extension of these studies (Alshammari et al., 2021; Aly et al., 2020, 2015; Mostafa et al., 2022), we present the synthesis of novel hybrid compounds based on pyrimidine and thiazole pharmacophores *via* the reaction of 3-substituted thiourea derivatives with 2-bromo-1-phenylethanone, 1-chloropropan-2-one, and ethyl bromoacetate. As a result, two new series of thiazolyl/pyrimidine-2,4-diones **3a-l** (Scaffold A) and thiazolidinylpyrimidine-2,4-diones **5a-e** (Scaffold B) were developed in the hope of obtaining new potent antiproliferative agents that can target EGFR and/or $BRAF^{V600E}$, as shown in Fig. 3.

All new compounds were tested for cell viability to see how they affected the viability of normal cell lines. The new compound will be tested as an antiproliferative agent against a panel of four cancer cell lines. Furthermore, the most active compounds will be tested against EGFR and $BRAF^{V600E}$ as potential targets for antiproliferative activity. Ultimately, docking computations were executed to reveal the docking pose of the most active compounds toward EGFR and $BRAF^{V600E}$ targets. The drug-likeness and ADMET characteristics were also anticipated for the investigated compounds.

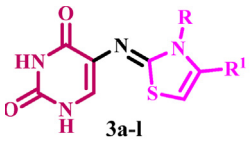

a: R = R^1 = Ph
b: R = 4-CH_3Ph, R^1 = Ph
c: R = 3-CH_3OPh, R^1 = Ph
d: R = CH_2Ph, R^1 = Ph
e: R = CH_3, R^1 = Ph
f: R = CH_2-CH=CH_2, R^1 = Ph
g: R = Ph, R^1 = CH_3
h: R = 4-CH_3Ph, R^1 = CH_3
i: R = 3-CH_3OPh, R^1 = CH_3
j: R = CH_2Ph, R^1 = CH_3
k: R = R^1 = CH_3
l: R = CH_2-CH=CH_2, R^1 = CH_3

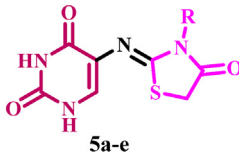

5a: R = Ph
5b: = 3-CH_3OPh
5c: = CH_2Ph
5d: = CH_3
5e: = CH_2-CH=CH_2

Fig. 3 Structure of new targets **3a-l** and **5a-e.**

2. Experimental (instruments in the Suppl. File)

2.1. Chemistry

General Details: Refer to Appendix A (Supplementary File).

Compounds **1a-e** and α-bromoacetophenone (**2a**) were synthesized according to the literature (Alshammari et al., 2022; Nobuta et al., 2010) Chloroacetone (**3b**) and ethyl 2-bromoacetate (**4**) were obtained from Aldrich.

2.1.1. General procedure for the synthesis of compounds 3a-l

Compounds **3a-l** were synthesized by refluxing thioureas **1a-e** (1 mmol) with α-bromoacetophenone (**2a**) and/or chloroace-

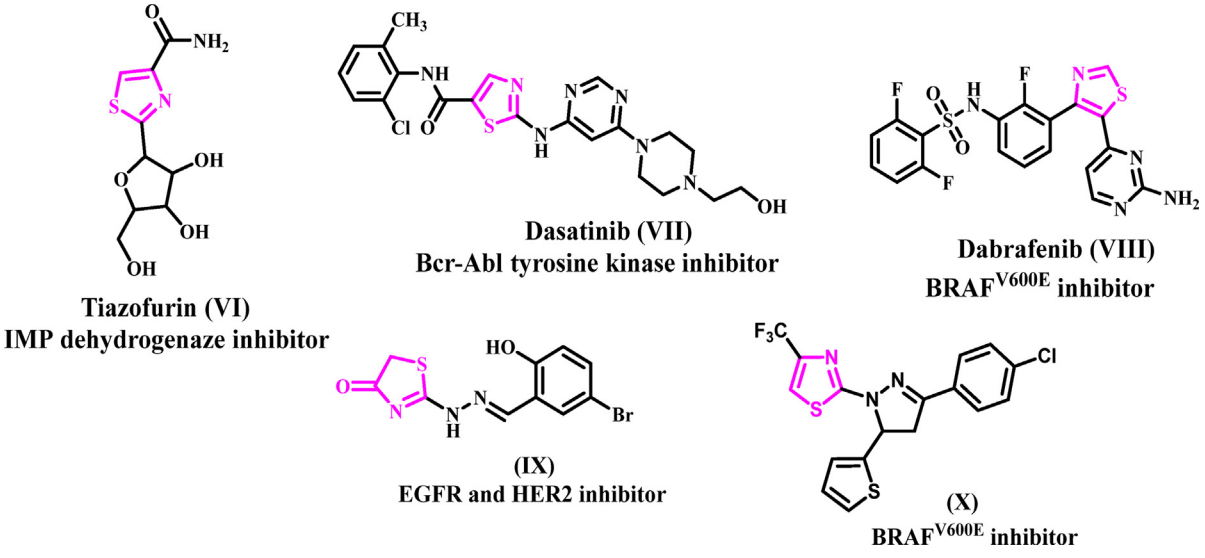

Fig. 2 Some clinically used thiazole-containing anti-cancer drugs **VI-VIII** and reported thiazole-based kinase inhibitors **IX** and **X**.

tone (**3b**) (1 mmol) in 50 mL of absolute ethanol as a solvent and the presence of few drops (0.5 mL) of triethylamine as a catalyst for 4–7 h. The resulting solid was filtered and recrystallized from DMF/EtOH (1:10).

2.1.1.1. (Z)-5-((3,4-Diphenylthiazol-2(3H)-ylidene)amino) pyrimidine-2,4(1H,3H)-dione (3a). Yield: 78 %; mp 314–316 °C, IR (KBr) υ_{max}/cm^{-1} = 3135 (NH), 3000 (Ar-CH), 1688–1680 (C═O), 1597 (C═N), 1558 (C═C). ^{1}H NMR (400 MHz, DMSO d_6): δ_H = 7.17 (s, 1H, CH-5′), 7.35–7.36 (m, 2H, H- Ar-H), 7.46–7.49 (m, 6H, Ar-H), 7.60 (dd, 2H, J = 7.7, 7.6 Hz, Ar-H), 8.32 (d, 1H, J = 6.3 Hz, H-6), 11.62 (br,d, 1H, J = 5.1 Hz, NH-1), 11.73 ppm (br,s, 1H, NH-3). ^{13}C NMR (100 MHz, DMSO d_6): δ_C = 104.7 (C-5′), 108.4 (C-5), 123.9, 128.3, 128.7, 129.2, 130.1 ppm (CH-Ar), 130.4, 142.0 (C-Ar), 143.1 (C-6), 146.0 (C-2′, 4′'), 150.6 (C-2), 160.2 ppm (C-4). MS (70 eV, %): m/z = 364 (M + 2, 15), 363 (M + 1, 62), 362 (M^+, 8), 285 (5), 255 (3), 154 (20), 102 (100). Anal. Calcd for $C_{19}H_{14}N_4O_2S$ (362.41): C, 62.97; H, 3.89; N, 15.46; S, 8.85. Found: C, 62.85; H, 3.92; N, 15.58; S, 8.94.

2.1.1.2. (Z)-5-((4-Phenyl-3-(p-tolyl)thiazol-2(3H)-ylidene) amino)pyrimidine-2,4(1H,3H)-dione (3b). Yield: 74 %; mp 306–308 °C, IR (KBr): υ_{max}/cm^{-1} = 3135 (NH), 3000 (Ar-CH), 1688–1670 (C═O), 1597 (C═N), 1558 (C═C). ^{1}H NMR (400 MHz, DMSO d_6): δ_H = 2.38 (s, 3H, CH_3), 7.18 (s, 1H, CH-5′), 7.34–7.36 (m, 4H, H-*o*, *o*'), 7.39–7.41 (m, 2H, H-*m*), 7.46–7.49 (m, 3H, *H-m', p'*), 8.32 (d, 1H, J = 6.3 Hz, H-6), 11.62 (d, 1H, J = 5.7 Hz, NH-1), 11.73 ppm (br,s, 1H, NH-3). ^{13}C NMR (100 MHz, DMSO d_6) δ_C = 20.66 (CH_3), 104.97 (C-5′), 108.20 (C-5), 123.91 (C-*o*), 128.25 (C-i'), 128.70 (C-*m*'), 129.22 (C-*o*'), 130.13 (C-*p*'), 130.86 (C-*m*), 138.20 (C-*p*), 142.01 (C-6, C-*i*), 146.07 (C-2′, C-4′), 150.58 (C-2), 160.16 ppm (C-4). MS (70 eV, %): m/z = 378 (M + 2, 27), 377 (M + 1, 100), 376 (M^+, 15), 372 (10), 283 (5), 255 (5), 154 (25), 136 (17), 102 (83). Anal. Calcd for $C_{20}H_{16}N_4O_2S$ (376.43): C, 63.81; H, 4.28; N, 14.88; S, 8.52. Found: C, 63.92; H, 4.31; N, 14.98; S, 8.67.

2.1.1.3. (Z)-5-((3-(3-Methoxyphenyl)-4-phenylthiazol-2(3H)-ylidene)amino)-pyrimidine-2,4(1H,3H)-dione (3c). Yield: 76 %; mp 310–312 °C, IR (KBr) υ_{max}/cm^{-1} = 3188 (NH), 3055 (Ar-CH), 1679–1670 (C═O), 1607 (C═N), 1555 (C═C). ^{1}H NMR (400 MHz, DMSO d_6): δ_H = 3.81 (s, 3H, OCH_3), 6.96–7.01 (m, 3H, Ar-H), 7.13 (s, 1H, C-5′), 7.35–7.36 (m, 2H, H-*o*, *o*'), 7.47–7.49 (m, 4H, Ar-H), 8.26 (d, 1H, J = 6.0 Hz, H-6), 11.60 (d, 1H, J = 4.0 Hz, NH-1), 11.70 ppm (br,s, 1H, NH-3). ^{13}C NMR (100 MHz, DMSO d_6): δ_C = 55.5 (OCH_3), 108.6 (C-5′), 109.1 (C-5), 113.7 (C-*o*), 115.4 (C-*o*'), 128.7 (C-*i*'), 128.8 (C-*m*'), 129.2 (C-*p*'), 130.0 (C-*m*'), 131.3 (C-*p*), 138.2 (C-*i*), 141.8 (C-6), 145.9 (C-4′), 150.6 (C-2′), 160.2 (C-2), 160.5 ppm (C-4). MS (70 eV, %): m/z = 394 (M + 2, 26), 393 (M + 1, 100), 392 (M^+, 10), 289 (5), 154 (17), 136 (13). Anal. Calcd for $C_{20}H_{16}N_4O_3S$ (392.43): C, 61.21; H, 4.11; N, 14.28; S, 8.17. Found: C, 61.35; H, 4.15; N, 14.40; S, 8.28.

2.1.1.4. (Z)-5-((3-Benzyl-4-phenylthiazol-2(3H)-ylidene) amino)pyrimidine-2,4(1H,3H)-dione (3d). Yield: 75 %; mp 312–314 °C, IR (KBr) υ_{max}/cm^{-1} = 3135 (NH), 3000 (Ar-CH), 1678–1670 (C═O), 1600 (C═N), 1556 (C═C). ^{1}H NMR (400 MHz, DMSO d_6): δ_H = 5.28 (s, 2H, NCH_2), 6.95–7.00 (m, 3H, Ar-H), 7.25–7.30 (m, 5H, Ar-H + H-5′), 7.35–7.49 (m, 3H, Ar-H), 7.58 (s, 1H, H-6), 11.19 (br,s, 1H, NH-1), 11.56 ppm (br,s, 1H, NH-3). ^{13}C NMR (100 MHz, DMSO d_6): δ_C = 45.7 (NCH_2), 104.2 (CH-5′), 108.6 (C-5), 126.6, 127.4, 127.6, 128.2, 128.5, 128.7, 129.3, 129.9 (CH-Ar), 132.2, 138.2 (C-Ar), 141.8 (C-6), 146.2 (C-4′), 148.2 (C-2′), 150.5 (C-2), 160.2 ppm (C-4). MS (70 eV, %): m/z = 376 (M^+, 100), 283 (14), 255 (10), 154 (15), 136 (10), 102 (40). Anal. Calcd for $C_{20}H_{16}N_4O_2S$ (376.43): C, 63.81; H, 4.28; N, 14.88; S, 8.52. Found: C, 63.94; H, 4.31; N, 14.98; S, 8.61.

2.1.1.5. (Z)-5-((3-Methyl-4-phenylthiazol-2(3H)-ylidene) amino)pyrimidine-2,4(1H,3H)-dione (3e). Yield: 78 %; mp 308–310 °C, IR (KBr) υ_{max}/cm^{-1} = 3142 (NH), 3055 (Ar-CH), 1668–1660 (C═O), 1598 (C═N), 1578 (C═C). ^{1}H NMR (400 MHz, DMSO d_6): δ_H = 3.32 (s, 3H, NCH_3), 6.51 (s, 1H, CH-5′), 7.27 (d, 1H, J = 4.0 Hz, H-6), 7.52–7.58 (m, 5H, Ar-H), 10.78 (br,s, 1H, NH-1), 11.29 ppm (br,s, 1H, NH-3). ^{13}C NMR (100 MHz, DMSO d_6): δ_C = 33.6 (NCH_2), 99.1 (C-5′), 108.3 (C-5), 128.8, 128.9, 129.4 (CH-Ar), 138.3 (C-Ar), 140.6 (C-6), 142.3 (C-4′), 148.6 (C-2′), 150.5 (C-2), 160.4 ppm (C-4). MS (70 eV, %): m/z = 300 (M^+, 13), 289 (10), 255 (10), 154 (48), 102 (100). Anal. Calcd for $C_{14}H_{12}N_4O_2S$ (300.34): C, 55.99; H, 4.03; N, 18.65; S, 10.68. Found: C, 55.88; H, 4.07; N, 18.78; S, 10.77.

2.1.1.6. (Z)-5-((3-Allyl-4-phenylthiazol-2(3H)-ylidene) amino)pyrimidine-2,4(1H,3H)-dione (3f). Yield: 74 %; mp 304–306 °C, IR (KBr) υ_{max}/cm^{-1} = 3297 (NH), 3089 (Ar-CH), 1675–1665 (C═O), 1656 (C═N), 1582 (C═C). ^{1}H NMR (400 MHz, DMSO d_6): δ_H = 4.15 (d, 2H, J = 8 Hz, N-CH_2), 5.08 (d, 1H, J = 10.1 Hz, H-3′c), 5.18 (dd, 1H, J = 17.2, 1.1 Hz, H-3′c), 5.83 (ddt, 1H, J_d = 17.2, 10.4 Hz, J_t = 5.2 Hz, H-3b), 7.14–7.18 (m, 2H, Ar-H), 7.25–7.31 (m, 3H, Ar-H), 8.89 (s, 1H, H-6), 11.34 (br,s, 1H, NH-1), 11.66 ppm (br,s, 1H, NH-3). ^{13}C NMR (100 MHz, DMSO d_6): δ_C = 45.7 (N-CH_2), 107.0 (C-5′), 110.0 (C-5), 116.5 (C-3′c), 131.7 (C-3′b), 127.1, 127.5, 128.7, 129.2, 129.9 (CH-Ar), 131.2 (C-Ar), 140.5 (C-6), 142.2 (C-4′), 148.1 (C-2′), 150.4 (C-2), 160.2 ppm (C-4). MS (70 eV, %): m/z = 326 (M^+, 50), 283 (9), 255 (10), 154 (25), 136 (15), 102 (100). Anal. Calcd for $C_{16}H_{14}N_4O_2S$ (326.37): C, 58.88; H, 4.32; N, 17.17; S, 9.82. Found: C, 55.96; H, 4.36; N, 17.28; S, 9.94.

2.1.1.7. (Z)-5-((4-Methyl-3-phenylthiazol-2(3H)-ylidene) amino)pyrimidine-2,4(1H,3H)-dione (3g). Yield: 74 %; mp 302–304 °C, IR (KBr) υ_{max}/cm^{-1} = 3172 (NH), 3017 (Ar-CH), 1676–1660 (CO), 1605 (C═N), 1597 (C═C). ^{1}H NMR (400 MHz, DMSO d_6): δ_H = 2.21 (s, 3H, CH_3), 6.10 (s, 1H, CH-5′), 7.15–7.21 (m, 5H, H- Ar-H), 8.05 (s, 1H, H-6), 10.86 (br,s, 1H, NH-1), 11.36 ppm (br,s, 1H, NH-3). ^{13}C NMR (100 MHz, DMSO d_6) δ_C = 20.4 (CH_3), 104.1 (C-5′), 113.3 (C-5), 125.3, 128.2, 128.9 (CH-Ar), 137.3 (C-Ar), 140.2 (C-6), 143.7 (C-4′), 148.3 (C-2′), 150.0 (C-2), 161.4 ppm (C-4). MS (70 eV, %): m/z = 300 (M^+, 85), 283 (10), 239 (40), 102 (100). Anal. Calcd for $C_{14}H_{12}N_4O_2S$ (300.34): C, 55.99; H, 4.03; N, 18.65; S, 10.68. Found: C, 55.88; H, 4.07; N, 18.78; S, 10.77.

2.1.1.8. (Z)-5-((4-Methyl-3-(p-tolyl)thiazol-2(3H)-ylidene) amino)pyrimidine-2,4(1H,3H)-dione (3h). Yield: 75 %; mp 312–314 °C, IR (KBr) υ_{max}/cm^{-1} = 3145 (NH), 3000 (Ar-CH), 1668–1660 (C═O), 1600 (C═N), 1547 (C═N). ^{1}H

NMR (400 MHz, DMSO d_6): δ_H = 1.88 (s, 3H, CH_3), 2.24 (s, 3H, CH_3), 5.92 (s, 1H, CH-5′), 6.75 (d, 2H, J = 8.0 Hz, Ar-H), 7.06 (d, 2H, J = 8.0 Hz, Ar-H), 7.90 (d, 1H, J = 7.6 Hz, H-6), 11.30 (d, 1H, J = 7.6 Hz, NH-1), 11.50 ppm (br,s, 1H, NH-3). ^{13}C NMR (100 MHz, DMSO d_6): δ_C = 18.2 (CH_3), 20.4 (CH_3), 95.0 (C-5′), 108.9 (C-5), 120.7, 129.6, 129.8 (CH-Ar), 134.9, 138.5 (C-Ar), 142.6 (C-6), 148.2 (C-2′, C-4′), 150.9 (C-2), 160.2 ppm (C-4). MS: m/z = 314 (M^+, 100), 295 (15), 273 (5), 242 (5), 167 (10). Anal. Calcd for $C_{15}H_{14}N_4O_2S$ (314.36): C, 57.31; H, 4.49; N, 17.82; S, 10.20. Found: C, 57.42; H, 4.52; N, 17.85; S, 10.29.

2.1.1.9. (Z)-5-((3-(3-Methoxyphenyl)-4-methylthiazol-2(3H)-ylidene)amino)pyrimidine-2,4(1H,3H)-dione (3i). Yield: 75 %; mp 308–310 °C, IR (KBr) υ_{max}/cm^{-1} = 3168 (NH), 3015 (Ar-CH), 1691–1668 (C═O), 1601 (C═N), 1545 (C═C). ^{1}H NMR (400 MHz, DMSO d_6): δ_H = 1.92 (s, 3H, CH_3), 3.76 (s, 3H, OCH_3), 5.99 (s, 1H, CH-5′), 6.72 (d, 1H, J = 8.0 Hz, Ar-H), 7.02 (d, 1H, J = 8.0 Hz, Ar-H), 7.22–7.26 (m, 2H, Ar-H), 8.10 (d, 1H, J = 7.6 Hz, H-6), 11.45 (d, 1H, J = 7.6 Hz, NH-1), 11.62 ppm (br,s, 1H, NH-3). ^{13}C NMR (100 MHz, DMSO d_6): δ_C = 19.1 (CH_3), 53.6 (CH_3), 95.1 (C-5′), 108.8 (C-5), 117.8, 125.1, 128.7, 129.4 (CH-Ar), 138.1, 139.6 (C-Ar), 142.5 (C-6), 146.2 (C-2′), 149.0 (C-4′), 151.0 (C-2), 161.2 ppm (C-4). MS (70 eV, %): m/z = 330 (M^+, 32), 302 (10), 263 (5), 154 (100), 136 (68). Anal. Calcd for $C_{15}H_{14}N_4O_3S$ (330.36): C, 54.53; H, 4.27; N, 16.96; S, 9.71. Found: C, 54.65; H, 4.30; N, 16.88; S, 9.82.

2.1.1.10. (Z)-5-((3-Benzyl-4-methylthiazol-2(3H)-ylidene)amino)pyrimidine-2,4(1H,3H)-dione (3j). Yield: 76 %; mp 315–317 °C, IR (KBr) υ_{max}/cm^{-1} = 3232 (NH), 3012 (Ar-CH), 1680–1663 (C═O), 1614 (C═N), 1568 (C═C). ^{1}H NMR (400 MHz, DMSO d_6): δ_H = 2.15 (s, 3H, CH_3), 5.02 (s, 2H, NCH_2), 5.88 (s, 1H, CH-5′), 7.27–7.45 (m, 5H, Ar-H), 7.57 (s, 1H, H-6), 11.40 (s, 1H, NH-1), 11.62 ppm (br,s, 1H, NH-3). ^{13}C NMR (100 MHz, DMSO d_6): δ_C = 18.2 (CH_3), 52.6 (NCH_2), 99.2 (C-5′), 108.7 (C-5), 127.6, 128.0, 128.6 (CH-Ar), 132.0 (C-Ar), 142.6 (C-6), 146.4 (C-2′), 149.0 (C-4′), 151.0 (C-2), 161.2 ppm (C-4). MS (70 eV, %): m/z = 314 (M^+, 100), 289 (15), 273 (5), 242 (5), 195 (10), 154 (40), 107 (23). Anal. Calcd for $C_{15}H_{14}N_4O_2S$ (314.36): C, 57.31; H, 4.49; N, 17.82; S, 10.20. Found: C, 57.43; H, 4.52; N, 17.91; S, 10.31.

2.1.1.11. (Z)-5-((3,4-Dimethylthiazol-2(3H)-ylidene)amino)pyrimidine-2,4(1H,3H)-dione (3k). Yield: 77 %; mp 306–308 °C, IR (KBr) υ_{max}/cm^{-1} = 3210 (NH), 1672–1665 (CO), 1608 (C═N), 1576 (C═C). ^{1}H NMR (400 MHz, DMSO d_6): δ_H = 2.16 (s, 3H, CH_3), 3.47 (s, 3H, CH_3), 6.32 (s, 1H, CH-5′), 7.36 (s, 1H, H-6), 10.97 (br,s, 1H, NH-1), 11.32 ppm (br, s, 1H, NH-3). ^{13}C NMR (100 MHz, DMSO d_6): δ_C = 13.9 (CH_3), 32.1 (NCH_3), 97.3 (C-5′), 119.3 (C-5), 134.6 (C-6), 137.3 (C-4′), 150.4 (C-2′), 160.4 (C-2), 166.2 ppm (C-4). MS (70 eV, %): m/z = 240 (M + 2, 7), 239 (M + 1, 56), 238 (M^+, 10), 168 (5), 154 (30), 136 (20), 102 (100). Anal. Calcd for $C_9H_{10}N_4O_2S$ (238.27): C, 45.37; H, 4.23; N, 23.51; S, 13.46. Found: C, 45.46; H, 4.27; N, 23.64; S, 13.55.

2.1.1.12. (Z)-5-((3-Allyl-4-methylthiazol-2(3H)-ylidene)amino)pyrimidine-2,4(1H,3H)-dione (3l). Yield: 74 %; mp 298–300 °C, IR (KBr) υ_{max}/cm^{-1} = 3211 (NH), 1677–1665 (C═O), 1648 (C═N), 1595 (C═C). ^{1}H NMR (400 MHz, DMSO d_6): δ_H = 2.18 (CH_3), 4.55 (d, 2H, J = 12.0 Hz, N-CH_2), 4.99 (d, 1H, J = 18.0 Hz, H-3′c), 5.10 (dd, 1H, J = 16.0, 1.1 Hz, H-3′c), 5.94 (ddt, 1H, Jd = 8.0 Hz, 12.0 Hz, Jt = 4.0 Hz, H-3b), 6.05 (s, 1H, CH-5′), 11.25 (br, s, 1H, NH-1), 11.37 ppm (br, s, 1H, NH-3). ^{13}C NMR (100 MHz, DMSO d_6): δ_C = 13.6 (CH_3), 45.3 (N-CH_2), 110.1 (C-5′), 117.0 (C-5), 117.9 (C-3′c), 130.6 (C-3′b), 131.5 (C-6), 137.1 (C-4′), 148.8 (C-2′), 150.4 (C-2), 160.2 ppm (C-4). MS (70 eV, %): m/z = 266 (M + 2, 17), 265 (M + 1, 100), 264 (M^+, 14), 224 (7), 165 (5), 154 (32), 136 (24), 102 (14). Anal. Calcd for $C_{11}H_{12}N_4O_2S$ (264.30): C, 49.99; H, 4.58; N, 21.20; S, 12.13. Found: C, 49.89; H, 4.61; N, 21.28; S, 12.21.

2.1.2. General procedure for the synthesis of compounds 5a-e

Compounds **5a-e** were synthesized by refluxing thioureas **1a-e** (1 mmol) with ethyl 2-bromo-acetate (**4**) (0.167 g, 1 mmol) in 30 mL of absolute ethanol as a solvent and the presence of few drops (0.5 mL) of triethylamine (Et_3N) as a catalyst for 6–8 h. The resulting solid was filtered and recrystallized from DMF/EtOH.

2.1.2.1. (Z)-5-((4-Oxo-3-phenylthiazolidin-2-ylidene)amino)pyrimidine-2,4(1H,3H)-dione (5a). Yield: 78 %; mp 298–300 °C, IR (KBr) υ_{max}/cm^{-1} = 3205 (NH), 3005 (Ar-CH), 1690–1675 (C═O), 1648 (C═N). ^{1}H NMR (400 MHz, DMSO d_6): δ_H = 4.05 (s, 2H, CH_2), 7.17 (d, 1H, J = 5.5 Hz, H-6), 7.32–7.40 (m, 5H, Ar-H), 11.50 ppm (br,s, 1H, NH-1), 11.75 ppm (br,s, 1H, NH-3). ^{13}C NMR (100 MHz, DMSO d_6): δ_C = 32.6 (CH_2), 106.6 (C-5), 127.4, 127.7, 128.0, 128.3 (CH-Ar), 135.7 (C-Ar), 144.4 (C-6), 150.5 (C-2), 159.8 (C-4), 170.5 ppm (C-4′). MS (70 eV, %): m/z = 302 (M^+, 60), 288 (10), 154 (15), 102 (100). Anal. Calcd for $C_{13}H_{10}N_4O_3S$ (302.31): C, 51.65; H, 3.33; N, 18.53; S, 10.61. Found: C, 51.77; H, 3.37; N, 18.62; S, 10.73.

2.1.2.2. (Z)-5-((3-(3-Methoxyphenyl)-4-oxothiazolidin-2-ylidene)amino)pyrimidine-2,4(1H,3H)-dione (5b). Yield: 76 %; mp 306–308 °C, IR (KBr) υ_{max}/cm^{-1} = 3204 (NH), 3002 (Ar-CH), 1690–1676 (C═O), 1640 (C═N). ^{1}H NMR (400 MHz, DMSO d_6): δ_H = 3.64 (s, 3H, CH_3), 4.10 (s, 2H, CH_2), 6.88–6.92 (m, 2H, Ar-H), 7.17–7.22 (m, 2H, Ar-H), 7.64 (d, 1H, J = 5.4 Hz, H-6), 11.52 (br,s, 1H, NH-1), 11.70 ppm (br,s, 1H, NH-3). ^{13}C NMR (100 MHz, DMSO d_6): δ_C = 33.8 (CH_2), 108.1 (C-5), 125.2, 126.4, 128.1, 129.2 (CH-Ar), 131.3, 138.6 (C-Ar), 144.3 (C-6), 150.8 (C-2), 158.6 (C-4), 171.0 ppm (C-4′). MS (70 eV, %): m/z = 304 (M + 2, 17), 303 (M + 1, 80), 302 (M^+, 13), 225 (15), 190 (12), 177 (100). Anal. Calcd for $C_{14}H_{12}N_4O_4S$ (302.31): C, 50.60; H, 3.64; N, 16.86; S, 9.65. Found: C, 50.61; H, 3.67; N, 16.99; S, 9.73.

2.1.2.3. (Z)-5-((3-Benzyl-4-oxothiazolidin-2-ylidene)amino)pyrimidine-2,4(1H,3H)-dione (5c). Yield: 79 %; mp 314–316 °C, IR (KBr) υ_{max}/cm^{-1} = 3152 (NH), 2974 (Ar-CH), 1689–1670 (CO), 1646 (C═N). ^{1}H NMR (400 MHz, DMSO d_6): δ_H = 4.11 (s, 2H, CH_2), 4.88 (s, 2H, NCH_2), 7.30–7.39 (m, 5H, Ar-H), 7.94 (d,1H, J = 8.0 Hz, H-6), 11.25 (br,s, 1H, NH-1), 11.50 ppm (br,s, 1H, NH-3). ^{13}C NMR (100 MHz, DMSO d_6): δ_C = 33.9 (CH_2), 45.4 (NCH_2), 106.6 (C-5), 127.8, 128.3, 128.6, 128.3 (CH-Ar), 136.0 (C-Ar), 138.1 (C-6), 144.7 (C-2′), 150.6 (C-2), 160.0 (C-4), 170.5 ppm (C-4′). MS (70 eV, %): m/z = 318

(M + 2, 20), 317 (M + 1, 100), 316 (M^+, 15), 232 (5), 178 (7), 155 (10), 154 (35), 136 (30), 102 (37), 91 (42). Anal. Calcd for $C_{14}H_{12}N_4O_3S$ (316.34): C, 53.16; H, 3.82; N, 17.71; S, 10.14. Found: C, 53.28; H, 3.85; N, 17.82; S, 10.22.

2.1.2.4. (Z)-5-((3-Methyl-4-oxothiazolidin-2-ylidene)amino) pyrimidine-2,4(1H,3H)-dione (5d). Yield: 76 %; mp 294–296 °C, IR (KBr) υ_{max}/cm^{-1} = 3168 (NH), 1687–1670 (C═O), 1650 (C═N), 1598 (C═C). ^{1}H NMR (400 MHz, DMSO d_6): δ_H = 4.04 (s, 2H, CH_2), 4.43 (d, 2H, J = 4.0 Hz, NCH_2), 5.19 (dd, 1H, J = 12.0 Hz, 1.0 Hz, H-3c'), 5.22 (dd, 1H, J = 12.0 Hz, 1.1 Hz, H-3c'), 5.90 (ddt, 1H, J_d = 17.1, 10.4 Hz, J_t = 5.1 Hz, H-3b'), 7.30 (d, 1H, J = 6.4 Hz, H-6), 11.14 (bd, 1H, J = 4.0 Hz, NH-1), 11.56 ppm (br,s, 1H, NH-3). ^{13}C NMR (100 MHz, DMSO d_6): δ_C = 35.14 (CH_2), 44.45 (NCH_2), 117.60 (C-3c'), 118.20 (C-5), 130.85 (C-3b'), 131.90 (C-6), 148.73 (C-2′), 150.60 (C-2), 160.05 (C-4), 172.10 ppm (C-4′). MS (70 eV, %): m/z = 240 (M^+, 100), 229 (5), 188 (34), 154 (10), 102 (80). Anal. Calcd for $C_8H_8N_4O_3S$ (240.24): C, 40.00; H, 3.36; N, 23.32; S, 13.35. Found: C, 40.09; H, 3.40; N, 23.43; S, 13.43.

2.1.2.5. (Z)-5-((3-Allyl-4-oxothiazolidin-2-ylidene)amino) pyrimidine-2,4(1H,3H)-dione (5e). Yield: 76 %; mp 296–298 °C, IR (KBr) υ_{max}/cm^{-1} = 3155 (NH), 1690–1668 (C═O), 1605 (C═N), 1545 (C═C). ^{1}H NMR (400 MHz, DMSO d_6): δ_H = 4.04 (s, 2H, CH_2), 4.43 (d, 2H, J = 4.0 Hz, NCH_2), 5.19 (dd, 1H, J = 12.0 Hz, 1.0 Hz, H-3c'), 5.22 (dd, 1H, J = 12.0 Hz, 1.1 Hz, H-3c'), 5.90 (ddt, 1H, J_d = 17.1, 10.4 Hz, J_t = 5.1 Hz, H-3b'), 7.30 (d, 1H, J = 6.4 Hz, H-6), 11.14 (b,d; 1H, J = 4.0 Hz, NH-1), 11.56 ppm (br,s, 1H, NH-3). ^{13}C NMR (100 MHz, DMSO d_6): δ_C = 35.1 (CH_2), 44.5 (NCH_2), 117.6 (C-3c'), 118.2 (C-5), 130.9 (C-3b'), 131.9 (C-6), 148.7 (C-2′), 150.6 (C-2), 160.1 (C-4), 172.1 ppm (C-4′). MS (70 eV, %): m/z = 268 (M + 2, 20), 267 (M + 1, 85), 266 (M^+, 14), 111 (15), 225 (10), 195 (10), 154 (100), 137 (66), 102 (20). Anal. Calcd for $C_{10}H_{10}N_4O_3S$ (266.28): C, 45.11; H, 3.79; N, 21.04; S, 12.04. Found: C, 45.23; H, 3.82; N, 21.11; S, 12.14.

2.2. Biology

2.2.1. Cell viability assay and evaluation of IC_{50}

2.2.1.1. MTT assay. The MTT assay was used to determine how the synthesized compounds affected the viability of the mammary epithelial normal cell line (MCF-10A) (Al-Wahaibi et al., 2020; Mohassab et al., 2021). See Appendix A (Supplementary file).

2.2.1.2. Antiproliferative test. To investigate the antiproliferative potential of compounds **3a-l** and **5a-e**, the MTT assay was carried out using various cancer cell lines following previously reported procedures (Al-Sanea et al., 2020). See Appendix A (Supplementary file).

2.2.1.3. EGFR inhibitory activity assay. The most effective antiproliferative derivatives (**3a**, **3c**, **3f**, **3i**, **5b** and **5c**) were investigated for their inhibitory activity against EGFR as a possible target for their antiproliferative activity (Abdel-Aziz et al., 2021, Mohamed et al., 2021). See Appendix A (Supplementary file).

2.2.1.4. BRAF kinase inhibitory assay. Compounds **3a**, **3c**, **3f**, **3i**, **5b** and **5d** were tested for their inhibitory activity against $BRAF^{V600E}$, and the results are shown as IC_{50} values (Gomaa et al., 2022; El-Sherief et al., 2019). See Appendix A (Supplementary file).

3. Results and discussion

3.1. Chemistry

The synthetic sequence for the novel potentially biologically active molecules **3a-l** and **5a-e** are depicted in Scheme 1. Compounds **3a-l** and **5a-e** were synthesized from previously reported 1-(2,4-dioxo-1,2,3,4-tetrahydropyrimidin-5-yl)thiour ea **1a-e** (Alshammari et al., 2022)**.** The new compounds were obtained by heating the compounds **1a-e** with α-bromoacetophenone (**2a**), chloroacetone (**2b**), and ethyl bromoacetate (**4**) in refluxing ethanol and in the presence of triethylamine as a catalyst. IR, NMR, mass spectra, and elemental analyses confirmed the structure of the isolated compounds. COSY, ^{1}H–^{13}C HSQC, and ^{1}H–^{13}C HMBC experiments were used to assign signals from skeletal atoms unambiguously.

For example, the IR spectrum of **3b** revealed absorption at υ_{max} = 3135 for NH, 1688–1670 for C═O, 1597 for C═N, and 1558 for C═C. ^{1}H NMR spectral data of the assigned compound **3b** was identified as (*Z*)-5-((4-phenyl-3-(*p*-tolyl) thiazol-2(3*H*)-ylidene)amino)-pyrimidine-2,4(1*H*,3*H*)-dione (**3b**, Fig. 4) revealed singlet signals at δ_H = 11.73, 11.62, 7.18 and 2.38 ppm due to NH-3, NH-1, H-5′ and CH_3, respectively. H-6 appeared as a doublet at δ_H = 8.32 ppm (J = 6.3 Hz). The aromatic hydrogens system appeared between δ_H = 7.36–7.49 ppm. ^{13}C NMR spectrum revealed represented signals at δ_C = 160.2, 150.2, 108.2, 105.0 and 20.7 ppm due to ^{4}C = O, ^{2}C = O, C-5, C-5′ and CH_3, respectively (Fig. 4). The *p*-tolyl methyl hydrogens (H-a) and carbon (C-a) are distinctive at δ_H = 2.38 and δ_C = 20.7 ppm. H-a gives COSY correlation with a 2H signal at δ_H = 7.39 ppm assigned as H-*m;* H-a also gives HMBC correlation with a tall, ^{13}C-H signal at δ_C = 130.9 ppm, assigned as C-*m,* and an *i*-carbon-H at δ_C = 138.2 ppm, assigned as C-*p*. C-*p* gives HMBC correlation with a 4H signal at δ_H = 7.36 ppm. As the only signal with an odd number of hydrogens, H-*p'* must appear at δ_H = 7.49 ppm. The hydrogens at δ_H = 7.36 ppm give HSQC correlation with carbons at δ_C = 129.2 and 124.0 ppm, and the hydrogens at δ_H = 7.49 give HSQC correlation with carbons at δ_C = 130.1 and 128.7 ppm. The line at δ_C = 130.1 is much smaller than that at δ_C = 128.7, so the line at δ_C = 130.1 ppm is assigned as C-*p';* on chemical-shift grounds, the up-field line at δ_C = 124.0 ppm is assigned as C-*o*. (See Fig. 4).

On reacting compounds **1a-e** with ethyl bromoacetate (**4**), a new series of 4-oxothiazolidin-2-ylidene)amino)pyrimidine-2,4(1*H*,3*H*)-diones **5a-e** as more analogs for biological testing, was produced. The structure of **5a-e** was determined using spectroscopic properties and elemental analyses. The Z-form of the obtained products was supported based on similar reactions between substituted thiosemicarbazides with α-bromoacetophenone and the X-ray structure of the obtained thiazole (Aly et al., 2019).

To rationalize our results, we choose compound **5d,** which is assigned as (*Z*)-5-((3-methyl-4-oxothiazolidin-2-ylidene)ami no)-pyrimidine-2,4(1*H*,3*H*)-dione (Fig. 5). Elemental analysis

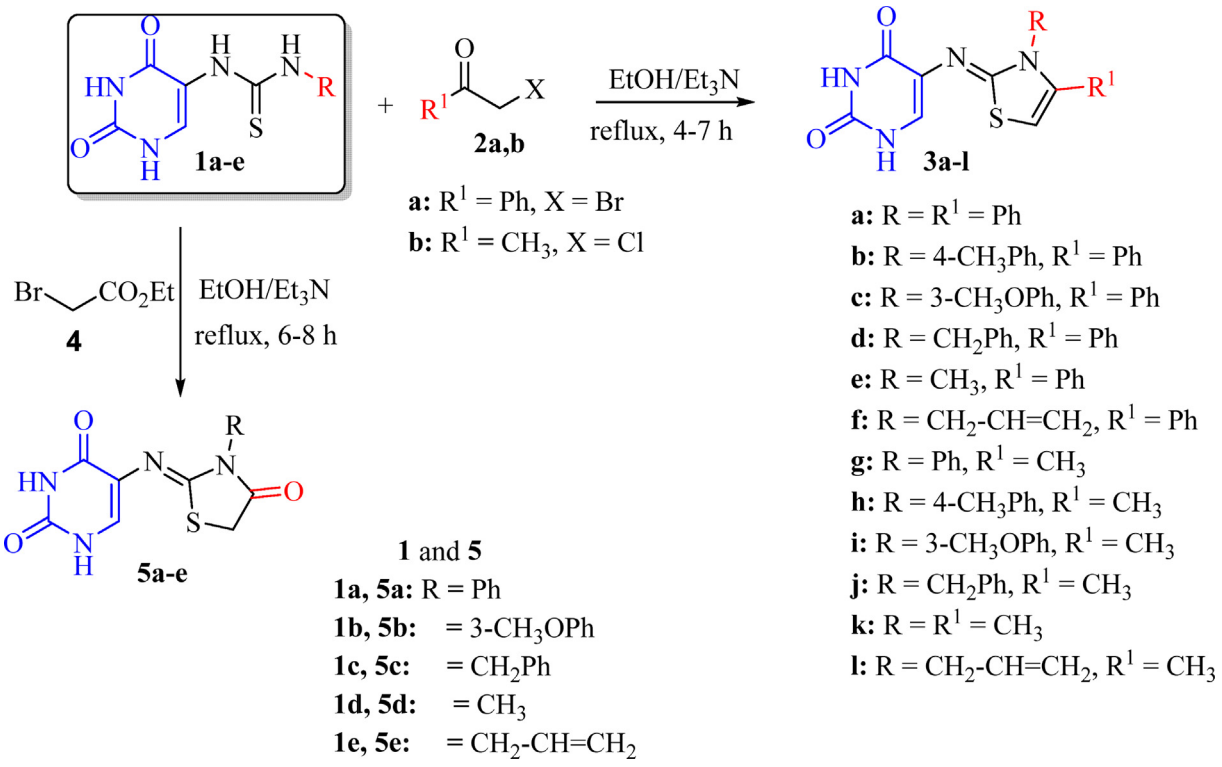

Scheme 1 Synthesis of uracil-based derivatives **3a-l** and **5a-e.**

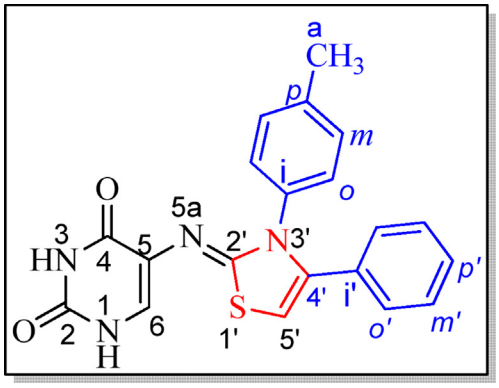

Fig. 4 Distinctive carbons and hydrogens for compound **3b.**

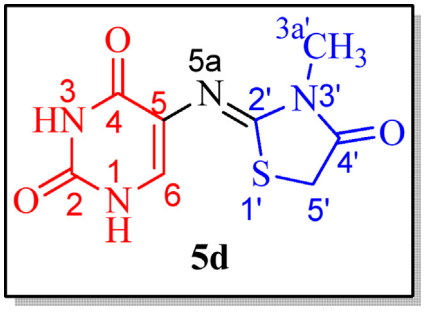

Fig. 5 Distinctive carbons and hydrogens for compound **5d.**

and mass spectrometry agreed with its general formula $C_8H_8N_4O_3S$ and molecular weight (m/z = 240). The IR spectrum of compound **5d** revealed absorptions of NH, C=O, C=N, and C=C at υ_{max} = 3168, 1687–1670, 1650, and 1598 cm^{-1}, respectively. The ^1H NMR spectrum for compound **5d** showed three-singlet signals at δ_H = 11.26 (1H), 4.05 (2H), and 3.11 ppm (3H), which they are assigned as NH-3, CH_2, and methyl (CH_3) group, respectively. Further, the H-6 and NH-1 are distinctive at δ_H = 7.07 and 10.72 ppm. The ^{13}C NMR spectrum of **5d** clearly showed the presence of CH_3 and CH_2 carbons of the thiazole ring, which resonated at δ_C = 29.1 and 32.7 ppm. Furthermore, the ^{13}C NMR spectrum revealed the presence of three carbonyl groups at δ_C = 172.1, 159.2, and 150.5 ppm for $^{5'}CO$, ^{4}CO, and ^{2}CO, respectively. At the same time, the (C-6 and C-2′) carbon atoms resonated at δ = 122.0 and 159.9 ppm, respectively, as can be observed in Fig. 5.

The mechanism describes the formation of compounds **3a-l** and **5a-e** due to the attack of the thione-lone pair on the α-bromo-C in **2a,b**, accompanied by elimination of a molecule of HX to give the intermediate **6** (Scheme 2). Subsequently, the cyclization process would occur *via* the internal nucleophilic attack of nitrogen lone-pair on the carbonyl carbon to give intermediates **7** (Scheme 2). Ultimately, a water molecule was eliminated from **7**, resulting in thiazole **3** (Scheme 2). Similarly, intermediate **8** would be formed from the reaction of **1a-e** with **4** and the elimination of the HX molecule. The cyclization step would be accompanied by the elimination of ethanol molecules to give compounds **5** (Scheme 2).

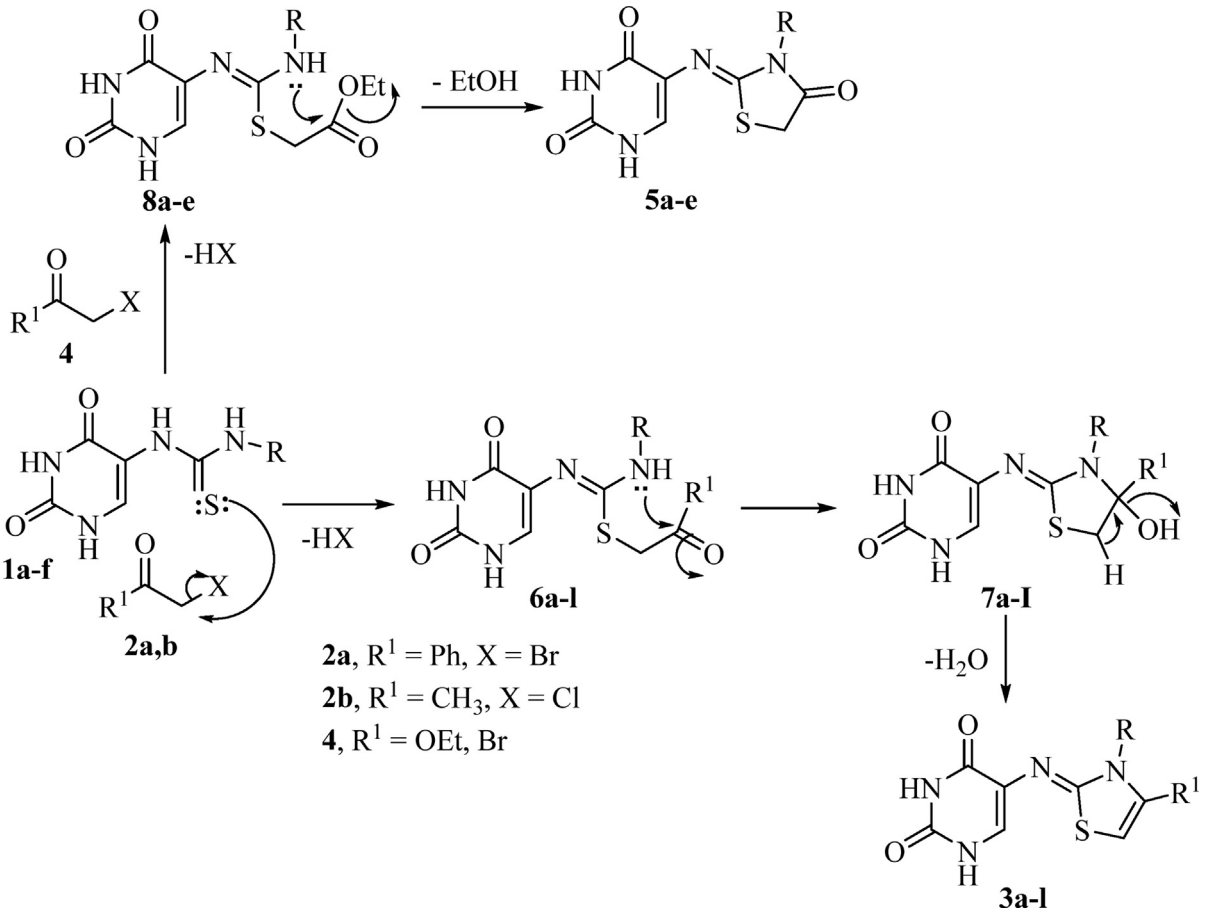

Scheme 2 The suggested mechanism for the formation of **3a-l** and **5a-e.**

3.2. Biology

3.2.1. Cell viability assay

The human mammary gland epithelial (MCF-10A) cell line was used to evaluate the viability of new compounds. Compounds **3a-l** and **5a-e** were incubated on MCF-10A cells for four days before the viability of the cells was assessed using the MTT assay (-Al-Wahaibi et al., 2020; Mohassab et al., 2021). Table 1 demonstrates that none of the compounds examined exhibited cytotoxic effects, and the cell viability for the compounds examined at 50 μM was greater than 87 %.

3.2.2. Antiproliferative assay

The antiproliferative activity of **3a-l** and **5a-e** was evaluated against the four human cancer cell lines Panc-1 (pancreatic cancer cell line), MCF-7 (breast cancer cell line), HT-29 (colon cancer cell line), and A-549 (lung cancer cell line) using the MTT assay (Al-Sanea et al., 2020) and doxorubicin as the reference drug. Table 1 displays the median inhibitory concentration (IC_{50}).

Overall, the antiproliferative activity of the compound examined was encouraging, with mean GI_{50} values against the four cancer cell lines ranging from 0.90 μM to 7.70 μM. The most potent derivatives were compounds **3a**, **3c**, **3f**, **3i**, and **5b** with GI_{50} values ranging from 0.90 μM to 1.70 μM. With a mean GI_{50} value of 0.90 μM against the four cancer cell lines, compound **3c** (R = *m*-CH_3O-Ph, R^1 = Ph) was the most effective derivative of the synthetic compounds compared to doxorubicin (GI_{50} = 1.10 μM). Compound **3c** was found to be more potent than doxorubicin against three of the four cancer cell lines tested, namely A-549 (lung cancer cell line), Panc-1 (pancreatic cancer cell line), and HT-29 (colon cancer cell line) while being equipotent to doxorubicin against MCF-7 (breast cancer) cell line.

Compound **3i** (R = *m*-CH_3O-Ph, R^1 = CH_3) ranks second in activity with a GI_{50} of 1.15 μM, matching the potency of doxorubicin (GI_{50} = 1.10 μM). Compound **3i** has the same structural backbone as **3c** except for the methyl group at position four of the thiazolidine ring moiety, indicating that the phenyl group, as in compound **3c**, is more tolerated for antiproliferative activity than the methyl group.

Compounds **3a** (R = Ph, R^1 = Ph) and **3b** (R = *p*-CH_3-Ph, R^1 = CH_3) showed promising antiproliferative activity, with GI_{50} values of 1.25 μM and 2.80 μM, respectively, being 1.4-fold and 3-fold less potent than **3c**. These findings show that the substitution pattern of the phenyl moiety in the third position of the thiazolidine ring is essential for antiproliferative action, with activity increasing in the order *m*-CH_3O- > H > *p*-CH_3-.

Compounds **3e** (R = CH_3, R^1 = Ph) and **3f** (R = CH_2 =-CH-CH_2–, R^1 = Ph) had GI_{50} values of 3.05 μM and 1.90 μM, respectively, and were less potent than **3a** (R = Ph, R^1 = Ph)

Table 1 IC_{50} of compounds **3a-l** and **5a-e** against four cancer cell lines.

Compound	Cell viability %	Antiproliferative activity IC_{50} ± SEM (μM)				
		A-549	MCF-7	Panc-1	HT-29	Average (GI_{50})
3a	**90**	1.20 ± 0.20	1.10 ± 0.10	1.40 ± 0.20	1.30 ± 0.20	1.25
3b	**89**	2.70 ± 0.30	2.60 ± 0.30	3.10 ± 0.30	2.90 ± 0.30	2.80
3c	**91**	0.80 ± 0.10	0.90 ± 0.10	1.00 ± 0.10	0.90 ± 0.10	0.90
3d	**91**	2.00 ± 0.20	1.90 ± 0.20	2.30 ± 0.20	2.20 ± 0.20	2.10
3e	**87**	2.90 ± 0.30	2.80 ± 0.30	3.30 ± 0.30	3.20 ± 0.30	3.05
3f	**89**	1.80 ± 0.20	1.60 ± 0.10	2.10 ± 0.20	2.10 ± 0.20	1.90
3 g	**91**	2.30 ± 0.20	2.10 ± 0.20	2.50 ± 0.20	2.40 ± 0.20	2.30
3 h	**92**	3.30 ± 0.30	3.10 ± 0.30	3.50 ± 0.30	3.60 ± 0.30	3.40
3i	**89**	1.10 ± 0.10	1.00 ± 0.10	1.30 ± 0.10	1.20 ± 0.10	1.15
3j	**87**	6.20 ± 0.60	6.00 ± 0.60	6.50 ± 0.60	6.40 ± 0.60	6.30
3 k	**90**	4.80 ± 0.50	4.70 ± 0.40	4.90 ± 0.50	4.90 ± 0.50	4.80
3 l	**87**	5.50 ± 0.60	5.30 ± 0.50	5.80 ± 0.60	5.70 ± 0.60	5.60
5a	**92**	2.40 ± 0.20	2.30 ± 0.20	2.80 ± 0.20	2.70 ± 0.20	2.55
5b	**90**	1.50 ± 0.10	1.60 ± 0.10	1.80 ± 0.20	1.80 ± 0.20	1.70
5c	**91**	1.40 ± 0.10	1.30 ± 0.10	1.60 ± 0.10	1.50 ± 0.10	1.45
5d	**87**	7.70 ± 0.70	7.50 ± 0.70	7.80 ± 0.80	7.90 ± 0.80	7.70
5e	**89**	7.00 ± 0.60	6.80 ± 0.70	7.30 ± 0.70	7.20 ± 0.70	7.10
Doxorubicin	–	1.20 ± 0.10	0.90 ± 0.10	1.40 ± 0.10	1.00 ± 0.10	1.10

indicating that un(substituted) phenyl ring is more tolerated for the antiproliferative action in the third position of thiazolidine moiety than allyl group and finally the methyl group. Compounds **3c** (R = *m*-CH_3O-Ph) and **3d** (R = CH_2-Ph) demonstrated great activity, with GI_{50} values of 1.70 μM and 1.45 μM, respectively, whereas compounds **3e** (R = CH_3) and **3f** (R = CH_2 = CH-CH_2–) were the least potent derivatives, with GI_{50} values of 7.70 μM and 7.10 μM, respectively.

3.2.3. EGFR inhibitory assay

The most effective antiproliferative derivatives (**3a**, **3c**, **3f**, **3i**, **5b** and **5c**) were investigated for their inhibitory activity against EGFR as a possible target for their antiproliferative activity (Abdel-Aziz et al., 2021; Mohamed et al., 2021). The findings are presented as IC_{50} values in Table 2. The results of this test are in line with those of antiproliferative assay, with compound **3c** (R = *m*-CH_3O-Ph, R^1 = Ph), the most potent antiproliferative derivative, demonstrating the highest inhibitory activity against EGFR with an IC_{50} value of 74 ± 07 nM, which is more potent than the reference erlotinib (IC_{50} = 80 ± 05 nM). Compound **3i** (R = *m*-CH_3O-Ph, R^1 = CH_3) is the second most active compound, with an IC_{50} value of 89 ± 08 nM, followed by compound **3a** (R = Ph, R^1 = Ph), which has an IC_{50} value of 97 ± 08 nM. The remaining compounds tested had lower activity, with an IC_{50} greater than 100 nM. After optimization, the results of this inhibitory assay test demonstrated that compounds 3c and 3i could be considered potent antiproliferative agents targeting EGFR.

Table 2 IC_{50} of compounds **3a**, **3c**, **3f**, **3i**, **5b**, and **5d** against EGFR and $BRAF^{V600E}$.

Compound	EGFR inhibition IC_{50} ± SEM (nM)	$BRAF^{V600E}$ inhibition IC_{50} ± SEM (nM)
3a	97 ± 08	138 ± 14
3c	74 ± 07	107 ± 10
3f	133 ± 13	167 ± 16
3i	89 ± 08	123 ± 12
5b	127 ± 13	159 ± 16
5d	115 ± 11	149 ± 15
Erlotinib	80 ± 05	60 ± 05

3.2.4. $BRAF^{V600E}$ inhibitory assay

Compounds **3a**, **3c**, **3f**, **3i**, **5b**, and **5d** were tested further for inhibitory activity against $BRAF^{V600E}$, and the results are shown in Table 2 as IC_{50} values (El-Sherief et al., 2019; Gomaa et al., 2022). Again, compound **3c** was found to be the most potent $BRAF^{V600E}$ inhibitor, with an IC_{50} value of 107 ± 10 nM, 1.8-fold less potent than the reference drug erlotinib (IC_{50} = 60 ± 05 nM).

Compounds **3i** and **3a** ranked second and third in activity with IC_{50} values of 123 ± 12 nM and 138 ± 14 nM, respectively. Considering the previous, we can be concluded that compounds **3c** and **3i** could be regarded as potent antiproliferative agents with dual inhibitory activity against EGFR and $BRAF^{V600E}$, though further structural modifications to develop more potent derivatives are required.

3.3. Molecular docking

The 3D structures of EGFR and $BRAF^{V600E}$ with PDB codes 1 M17 (Stamos et al., 2002) and 3OG7 (Bollag et al., 2010), respectively, were retrieved and utilized as templates for all docking predictions. All heteroatoms, ions, inhibitors, and water molecules were extracted to prepare the PDB files. All missing residues were built using Modeller software (Martí-Renom et al., 2000). The empirical program PropKa was utilized to assign the protonation state of residues of the investigated target (Olsson et al., 2011). The 3D structures of compounds **3a**, **3c** and **3i** were modeled using Omega2

software (Hawkins et al., 2010; OMEGA 2013). The generated structures were energetically minimized using the MMFF94S force field within SZYBKI software (Halgren, 1999; SZYBKI 2016).

AutoDock Vina1.1.2 (Trott and Olson, 2010) and AutoDock4.2.6 (Morris et al., 2009) software were used to execute all docking computations. The investigated targets were prepared as described elsewhere (Ibrahim et al., 2022, 2021b, 2021a). The docking parameters of AutoDock Vina1.1.2 and AutoDock4.2.6 software were generally kept at their default. For AutoDock Vina1.1.2 software, the exhaustiveness number was adjusted to 200. The grid box size was located at 19 Å × 19 Å × 19 Å. Besides, the grid spacing value was set to 1.0 Å. For AutoDock4.2.6 software, A maximum number of 25,000,000 energy evaluations and 250 independent docking runs were utilized. The grid box was tailored to fit the active site of EGFR and $BRAF^{V600E}$ proteins, with a grid size of 50 Å × 50 Å × 50 Å, with a spacing value of 0.375 Å. The grid center was positioned at the center of the active sites of EGFR and $BRAF^{V600E}$ proteins. The Gasteiger-Marsili method was employed to assign the atomic charges of these compounds (Gasteiger and Marsili, 1980). All molecular interactions were visualized using BIOVIA Discovery Studio Visualizer 2020 (Dassault Systèmes BIOVIA).

The binding features and scores of compounds **3a**, **3c**, and **3i** against EGFR and $BRAF^{V600E}$ were predicted using AutoDock Vina1.1.2 and AutoDock4.2.6 software. The anticipated binding scores and features of these compounds are summarized in Table 3. From data in Table 3, all investigated compounds demonstrated promising AutoDock scores against EGFR and BRAFV600E with values of − 8.9 to − 9.1 kcal/mol and − 8.4 to − 8.6 kcal/mol, respectively.

Compared to AutoDock scores, all investigated compounds demonstrated plausible Vina scores towards EGFR and $BRAF^{V600E}$ with values ranging from − 8.5 to − 8.7 kc al/mol and from − 7.2 to − 7.4 kcal/mol, respectively (Table 3). Notably, the binding modes predicted by AutoDock Vina1.1.2 software of the investigated compounds with the targets were very similar to those anticipated by AutoDock4.2.6 software. The good binding affinities of investigated compounds against EGFR and $BRAF^{V600E}$ may be attributed to their ability to exhibit H-bonds, pi-based, hydrophobic, and van der Waals interactions with the proximal amino acids inside the active sites of EGFR and $BRAF^{V600E}$. Compound **3c** revealed eminent AutoDock scores of − 9.1 and − 8.6 kcal/mol towards EGFR and $BRAF^{V600E}$, respectively (Table 3). More exactly, compound **3c** exhibited three hydrogen bonds with MET769 (1.96 Å), ARG817 (2.16 Å), and CYS773 (2.35 Å) and three hydrogen bonds with THR529 (3.30 Å), ILE527 (3.08 Å) and LYS483 (3.26 Å) inside the binding pockets of EGFR and $BRAF^{V600E}$, respectively (Figs. 6 and 7). Compound **3i** unveiled the second-lowest AutoDock score with values of − 9.0 and − 8.5 kcal/mol with EGFR and $BRAF^{V600E}$, respectively (Table 3). Inspecting the binding modes revealed that compound **3i** formed three and two hydrogen bonds with MET769 (1.96 Å), ARG817 (2.17 Å), and CYS773 (2.28 Å) and CYS532 (1.92, 2.07 Å) inside the binding pockets of EGFR and $BRAF^{V600E}$, respectively (Figs. 6 and 7).

Table 3 Computed Vina and AutoDock scores (kcal/mol) and binding features for compounds **3a**, **3c**, **3i**, and erlotinib towards EGFR and $BRAF^{V600E}$.

Compound	EGFR			$BRAF^{V600E}$		
	Vina Score (kcal/mol)	AutoDock Score (kcal/mol)	Binding features[a,b]	Vina Score (kcal/mol)	AutoDock Score (kcal/mol)	Binding features[a,b]
3a	−8.5	−8.9	CYS773 (2.31 Å), ARG817 (2.11 Å)	−7.2	−8.4	THR529 (3.17 Å), ALA481 (2.71 Å), ILE527 (2.84 Å)
3c	−8.7	−9.1	MET769 (1.96 Å), ARG817 (2.16 Å), CYS773 (2.35 Å)	−7.4	−8.6	THR529 (3.30 Å), ILE527 (3.08 Å), LYS483 (3.26 Å)
3i	−8.6	−9.0	MET769 (1.96 Å), ARG817 (2.17 Å), CYS773 (2.28 Å)	−7.3	−8.5	CYS532 (1.92, 2.07 Å)
Erlotinib	−7.9	−8.6	CYS773 (1.91 Å), MET769 (1.62 Å)	−7.0	−8.4	CYS532 (2.02 Å), THR529 (2.07 Å)

[a] Only conventional hydrogen bonds are listed.
[b] Binding features predicted by AutoDock4.2.6 software are listed.

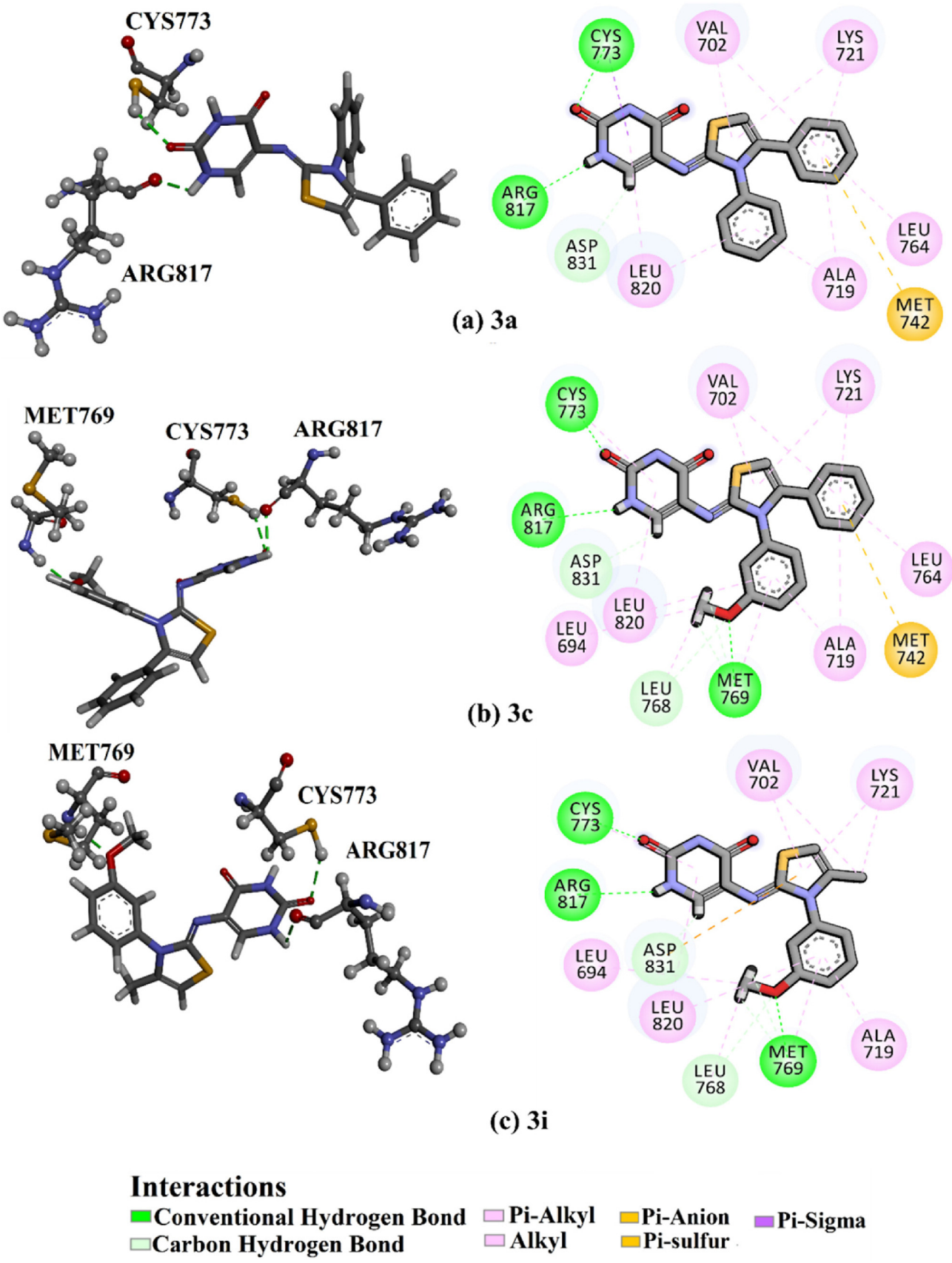

Fig. 6 3D and 2D molecular interactions of compounds (a) **3a**, (b) **3c**, and (c) **3i** with key residues of EGFR predicted by AutoDock4.2.6 software.

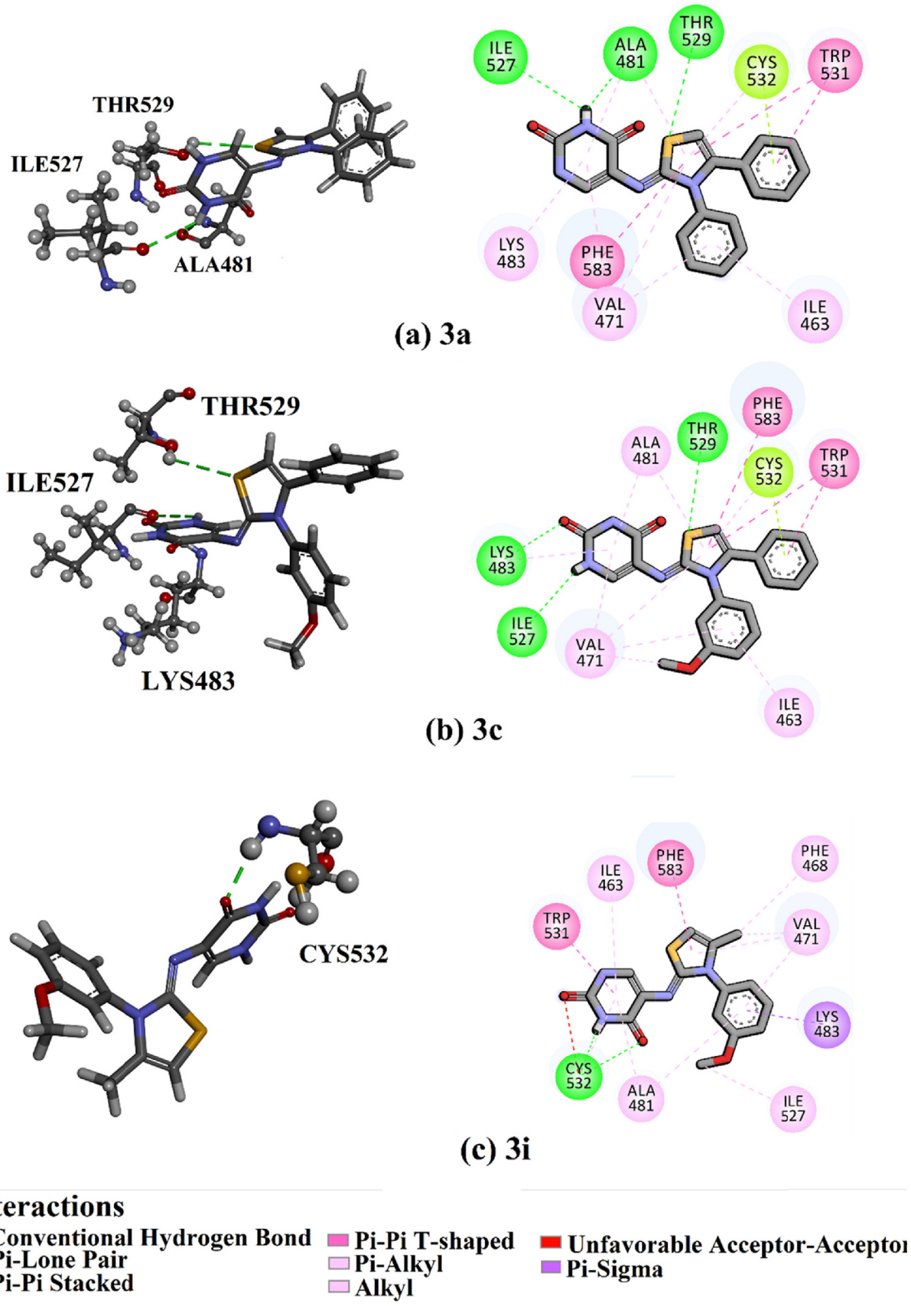

Fig. 7 3D and 2D molecular interactions of compounds (a) **3a**, (b) **3c**, and (c) **3i** with key residues of $BRAF^{V600E}$ predicted by AutoDock4.2.6 software.

As listed in Table 3, compound **3a** manifested good docking scores with values of − 8.9 and − 8.4 kcal/mol towards EGFR and $BRAF^{V600E}$, respectively. Notably, compound **3a** exhibited two and three hydrogen bonds with CYS773 (2.31 Å) and ARG817 (2.11 Å) and THR529 (3.17 Å), ALA481 (2.71 Å), and ILE527 (2.84 Å) inside the active sites of EGFR and $BRAF^{V600E}$, respectively (Table 3 and Fig. 6).

It is worth mentioning that compounds **3a**, **3c** and **3i** demonstrated pi-sulfur interaction with MET742 residue inside the active site of EGFR (Fig. 6). Besides, compound **3a** interacted with CYS773 by pi-sigma interaction within the binding site of EGFR (Fig. 6). On the other hand, compounds **3a**, **3c** and **3i** pi-lone pair with CYS532, pi-pi stacking with TRP531, and pi-pi T-shaped were noted with PHE583 amino acid within the binding pocket of $BRAF^{V600E}$ (Fig. 7).

Erlotinib, a positive control, exposed good docking scores against EGFR and $BRAF^{V600E}$ with values of − 8.6 and − 8.4 kcal/mol, respectively (Table 3). Erlotinib formed two hydrogen bonds with CYS773 (1.91 Å) and MET769 (1.62 Å) and two hydrogen bonds with CYS532 (2.02 Å) and THR529 (2.07 Å) within the binding pockets of EGFR and $BRAF^{V600E}$, respectively (Table 3). The current outcomes highlighted the importance of compounds **3a**, **3c**, and **3i** as potential antiproliferative agents.

3.4. ADMET study

Swiss ADME server was employed to predict the drug-likeness characteristics of compounds **3a**, **3c**, and **3i** (Daina et al., 2017). Under the framework of the Lipinski rule, five properties were deemed, involving the hydrogen bond acceptors (HBA $\leq$ 10), hydrogen bond donors (HBD $\leq$ 5), log *p*-value (log *p*0/w $\leq$ 5), molecular weight (MWt $\leq$ 500), and topological polar surface area (TPSA $\leq$ 140). Crossing these properties points out that the investigated compounds are orally bioavailable.

The absorption, distribution, metabolism, excretion, and toxicity (ADMET) properties for compounds **3a**, **3c**, and **3i** were estimated using a freely accessible web server pkCSM tool (Pires et al., 2015). Absorption (A) includes HIA (human intestinal absorption) and Caco-2 (human colorectal carcinoma) permeability. Distribution (D) is predicted by BBB (blood–brain barrier) permeability. The metabolism (M) is anticipated by CYP3A4 substrate/inhibitor. The excretion (E) and toxicity (T) were estimated by inhibitor total clearance and hepatotoxicity.

SwissADME server was utilized to predict the prospective character of compounds **3a**, **3c**, **3i** and erlotinib as drugs via evaluating the drug-likeness properties. The drug-likeness properties included MWt (g/mol), HBA, HBD, log p0/w, and TPSA ($Å^2$) (Table 4). As enrolled in Table 4, the MWts were 362.4, 392.4, 330.4, and 393.4 g/mol for compounds **3a**, **3c**, **3i** and erlotinib, respectively, allowing skin absorption. The number of HBA was < 10, and the number of HBA was < 5 (Table 4). Additionally, the Log P0/w values of compounds **3a**, **3c**, **3i**, and erlotinib were promising, with values < 5 (Table 4). The current results demonstrated that compounds **3a**, **3c**, **3i**, and erlotinib are promising inhibitors against EGFR and $BRAF^{V600E}$.

The knowledge of ADMET characteristics presents significant guidelines for starting stage drug discovery. HIA and Caco2 permeability must be deemed in any drug discovery process to anticipate the absorption property (Pires et al., 2015). The inspected compounds manifested good absorption with HIA values of 97.9 %, 89.1 %, 82.0 %, and 95.4 % for compounds **3a**, **3c**, **3i** and erlotinib, respectively (Table 4). Compounds **3a**, **3c**, and **3i**, exposed perfect Caco2 permeability with a value of < 0.9 cm/s. However, erlotinib showed poor Caco2 permeability with a value of 1.0 cm/s (Table 4). To examine drug distribution, the BBB membrane permeability was evaluated. Remarkable distribution volumes were observed for compounds **3a**, **3c**, **3i**, and erlotinib with log BB values of − 0.5, −0.9, −0.9 and − 0.6, respectively, demon-

Table 4 Predicted physiochemical and pharmacokinetic characteristics of compounds **3a**, **3c**, **3i**, and **erlotinib** as EGFR and $BRAF^{V600E}$ inhibitors.

Characteristics	3a	3c	3i	Erlotinib
Drug Likeness Properties				
MWt	362.4	392.4	330.4	393.4
HBD	2	2	2	1
HBA	3	4	4	6
log *p*0/w	2.6	1.9	0.9	1.9
TPSA	111.3	120.5	120.5	74.7
ADMET Properties				
Absorption (A)				
HIA	97.9 %	89.1 %	82.0 %	95.4 %
Caco2 Permeability	0.8	0.5	0.1	1.0
Distribution (D)				
BBB Permeability	−0.5	−0.9	−0.9	−0.6
Metabolism (M)				
CYP1A2 Inhibitor	Yes	Yes	No	No
Excretion (E)				
Total Clearance	−0.07	0.2	0.03	0.5
Toxicity (T)				
AMES toxicity	No	No	Yes	No

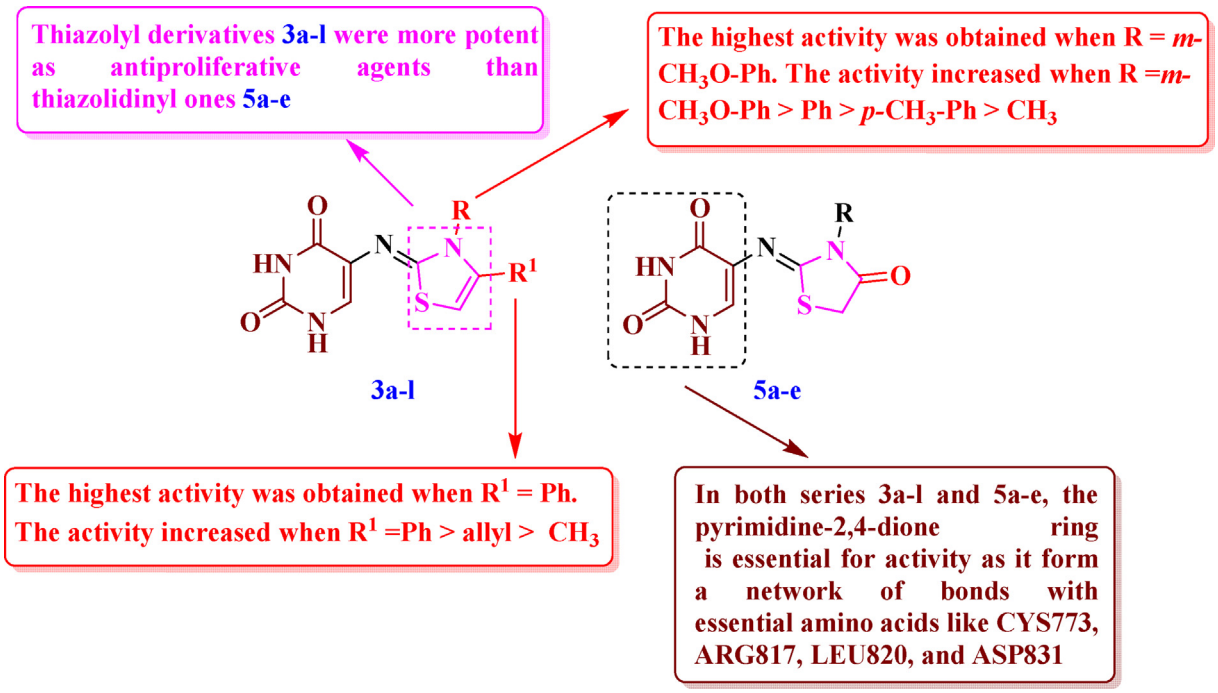

Fig. 8 SAR analysis of compounds **3a-l** and **5a-e.**

strating these compounds can cross BBB facilely (Table 4). CYP450 has an essential role in drug metabolism. The metabolism anticipations disclosed that compound **3i** and erlotinib could not inhibit CYP1A2 (Table 4). The total drug clearance was − 0.07, 0.2, 0.03, and 0.5 mL/min/kg for compounds **3a**, **3c**, **3i**, and erlotinib, respectively (Table 4). Toxicity plays a vital role in selecting drugs. Compounds **3a**, **3c**, and erlotinib did not demonstrate AMES toxicity; however, compound **3i** showed AMES toxicity (Table 4). These findings proved that compounds **3a**, **3c** and **3i** might be utilized as putative antiproliferative agents.

3.5. Structural activity relationship (SAR) analysis

The structural activity relationship of compounds **3a-l** and **5a-e** can be summarized in Fig. 8.

4. Conclusion

Due to the importance of thiazolyl pyrimidine derivatives, we direct for the synthesis of (Z)-5-((thiazol-2(3*H*)-ylidene)amino)pyrimidine-2, 4(1*H*,3*H*)-diones **3a-l** through the reaction of thioureas **1a-e** with α-bromoacetophenone (**2a**) and/or chloroacetone (**3b**). Similarly, thiazolidinones **5a-e** derived by uracil molecule were obtained *via* the reaction of **1a-e** with ethyl 2-bromoacetate. The structure of compounds was examined by ^{1}H, ^{13}C NMR, 2D NMR, and ^{15}N NMR spectroscopy and elemental analyses. The tested compounds displayed promising antiproliferative action, encouraging inhibitory activities against EGFR and/or BRAF^{V600E}. Moreover, the docking poses and scores of compounds **3a**, **3c**, and **3i** towards EGFR and BRAF^{V600E} were revealed using AutoDock4.2.6 software. Based on the docking scores, compounds **3a**, **3c** and **3i** displayed good docking scores towards EGFR and BRAF^{V600E}. Notably, the computed docking scores were in line with the IC_{50} values. Compounds **3a**, **3c** and **3i** also demonstrated excellent physicochemical and pharmacokinetic characteristics.

CRediT authorship contribution statement

Ashraf A. Aly: Conceptualization, Writing – original draft, Writing – review & editing. **M.B. Alshammari:** Editing and revision. **A. Ahmad:** Editing. **H.A.M. Gomaa:** Biology, Editing. **Bahaa G.M. Youssif:** Biology, Methodology, Writing – review & editing. **S. Bräse:** Editing and revision. **Mahmoud A.A. Ibrahim:** Writing – review & editing. **Asmaa H. Mohamed:** Conceptualization, Methodology, Writing – original draft.

Declaration of Competing Interest

The authors declare that they have no known competing financial interests or personal relationships that could have appeared to influence the work reported in this paper.

Acknowledgments

The authors thank the Deanship of Scientific Research at Prince Sattam bin Abdulaziz University under research project No 2021/01/18104. We also acknowledge support from the KIT-Publication Fund of the Karlsruhe Institute of Technology. Resources department at KIT for providing Prof Ashraf A. Aly with a two-month contract at the Karlsruhe Institute of Technology, Karlsruhe, Germany, from 2 August to 26 September 2022

Appendix A. Supplementary material

Supplementary data to this article can be found online at https://doi.org/10.1016/j.arabjc.2023.104612.

References

Abdel-Aziz, S.A., Taher, E.S., Lan, P., Asaad, G.F., Gomaa, H.A.M., El-Koussi, N.A., Youssif, B.G.M., 2021. Design, synthesis, and biological evaluation of new pyrimidine-5-carbonitrile derivatives bearing 1,3-thiazole moiety as novel anti-inflammatory EGFR inhibitors with cardiac safety profile. Bioorg. Chem. 111,. https://doi.org/10.1016/j.bioorg.2021.104890 104890.

Abdel-Maksoud, M.S., Kim, M.-R., El-Gamal, M.I., Gamal El-Din, M.M., Tae, J., Choi, H.S., Lee, K.-T., Yoo, K.H., Oh, C.-H., 2015. Design, synthesis, in vitro antiproliferative evaluation, and kinase inhibitory effects of a new series of imidazo[2,1-b]thiazole derivatives. Eur. J. Med. Chem. 95, 453–463. https://doi.org/10.1016/j.ejmech.2015.03.065.

Alam, M.M., Hassan, A.H.E., Kwon, Y.H., Lee, H.J., Kim, N.Y., Min, K.H., Lee, S.-Y., Kim, D.-H., Lee, Y.S., 2018. Design, synthesis and evaluation of alkylphosphocholine-gefitinib conjugates as multi-target anti-cancer agents. Arch. Pharm. Res. 41, 35–45. https://doi.org/10.1007/s12272-017-0977-z.

Alam, M.M., Hassan, A.H.E., Lee, K.W., Cho, M.C., Yang, J.S., Song, J., Min, K.H., Hong, J., Kim, D.-H., Lee, Y.S., 2019. Design, synthesis and cytotoxicity of chimeric erlotinib-alkylphospholipid hybrids. Bioorg. Chem. 84, 51–62. https://doi.org/10.1016/j.bioorg.2018.11.021.

Al-Sanea, M.M., Gotina, L., Mohamed, M.F.A., Parambi, D.G.T., Gomaa, H.A.M., Mathew, B., Youssif, B.G.M., Alharbi, K.S., Elsayed, Z.M., Abdelgawad, M.A., Eldehna, W.M., 2020. Design, synthesis and biological evaluation of new HDAC1 and HDAC2 inhibitors endowed with ligustrazine as a novel cap moiety. Drug Des. Devel. Ther. 14, 497–508. https://doi.org/10.2147/DDDT.S237957.

Alshammari, M.B., Aly, A.A., Youssif, B.G.M., Bräse, S., Ahmad, A., Brown, A.B., Ibrahim, M.A.A., Mohamed, A.H., 2022. Design and synthesis of new thiazolidinone/uracil derivatives as antiproliferative agents targeting EGFR and/or BRAFV600E. Front. Chem. https://doi.org/10.3389/fchem.2022.1076383.

Alshammari, M.B., Mohamed, A.H., Aly, A.A., Bakht, M.A., El-Sheref, E.M., 2021. New quinolin-3-yl-N-hydrazinecarbothioamides in the synthesis of thiazoles and thiazines. J. Sulfur Chem. 42, 346–357. https://doi.org/10.1080/17415993.2021.1887190.

Al-Wahaibi, L.H., Gouda, A.M., Abou-Ghadir, O.F., Salem, O.I.A., Ali, A.T., Farghaly, H.S., Abdelrahman, M.H., Trembleau, L., Abdu-Allah, H.H.M., Youssif, B.G.M., 2020. Design and synthesis of novel 2,3-dihydropyrazino[1,2-a]indole-1,4-dione derivatives as antiproliferative EGFR and BRAFV600E dual inhibitors. Bioorg. Chem. 104,. https://doi.org/10.1016/j.bioorg.2020.104260 104260.

Aly, A.A., Ishak, E.A., El Malah, T., Brown, A.B., Elayat, W.M., 2015. Synthesis of potentially antioxidant and antibacterial biologically active thiazolidines. J. Heterocycl. Chem. 52, 1758–1764. https://doi.org/10.1002/jhet.2248.

Aly, A.A., El-Sheref, E.M., Brown, A.B., Bräse, S., Nieger, M., Abdelhafez, E.-S.-M.-N., 2019. New one-pot synthesis of 2-ylidenehydrazono-thiazoles. J. Sulfur Chem. 40, 641–647. https://doi.org/10.1080/17415993.2019.1635132.

Aly, A.A., Mohamed, A.H., Ramadan, M., 2020. Synthesis and colon anti-cancer activity of some novel thiazole/-2-quinolone derivatives. J. Mol. Struct. 1207,. https://doi.org/10.1016/j.molstruc.2020.127798 127798.

Ayati, A., Emami, S., Asadipour, A., Shafiee, A., Foroumadi, A., 2015. Recent applications of 1,3-thiazole core structure in the identification of new lead compounds and drug discovery. Eur. J. Med. Chem. 97, 699–718. https://doi.org/10.1016/j.ejmech.2015.04.015.

Bai, S., Liu, S., Zhu, Y., Wu, Q., 2018. Asymmetric synthesis and antiviral activity of novel chiral amino-pyrimidine derivatives. Tetrahedron Lett. 59, 3179–3183. https://doi.org/10.1016/j.tetlet.2018.07.020.

Banerji, B., Chandrasekhar, K., Sreenath, K., Roy, S., Nag, S., Saha, K.D., 2018. Synthesis of triazole-substituted quinazoline hybrids for anticancer activity and a lead compound as the EGFR blocker and ROS inducer agent. ACS Omega 3, 16134–16142. https://doi.org/10.1021/acsomega.8b01960.

Beckers, T., Mahboobi, S., Sellmer, A., Winkler, M., Eichhorn, E., Pongratz, H., Maier, T., Ciossek, T., Baer, T., Kelter, G., Fiebig, H.-H., Schmidt, M., 2012. Chimerically designed HDAC- and tyrosine kinase inhibitors. A series of erlotinib hybrids as dual-selective inhibitors of EGFR, HER2 and histone deacetylases. Medchemcomm 3, 829–835. https://doi.org/10.1039/C2MD00317A.

Bollag, G., Hirth, P., Tsai, J., Zhang, J., Ibrahim, P.N., Cho, H., Spevak, W., Zhang, C., Zhang, Y., Habets, G., Burton, E.A., Wong, B., Tsang, G., West, B.L., Powell, B., Shellooe, R., Marimuthu, A., Nguyen, H., Zhang, K.Y.J., Artis, D.R., Schlessinger, J., Su, F., Higgins, B., Iyer, R., D'Andrea, K., Koehler, A., Stumm, M., Lin, P.S., Lee, R.J., Grippo, J., Puzanov, I., Kim, K.B., Ribas, A., McArthur, G.A., Sosman, J.A., Chapman, P.B., Flaherty, K.T., Xu, X., Nathanson, K.L., Nolop, K., 2010. Clinical efficacy of a RAF inhibitor needs broad target blockade in BRAF-mutant melanoma. Nature 467, 596–599. https://doi.org/10.1038/nature09454.

Borik, R.M., Fawzy, N.M., Abu-Bakr, S.M., Aly, M.S., 2018. Design, synthesis, anticancer evaluation and docking studies of novel heterocyclic derivatives obtained via reactions involving curcumin. Molecules 23, 1398. https://doi.org/10.3390/molecules23061398.

Cai, X., Zhai, H.-X., Wang, J., Forrester, J., Qu, H., Yin, L., Lai, C.-J., Bao, R., Qian, C., 2010. Discovery of 7-(4-(3-Ethynylphenylamino)-7-methoxyquinazolin-6-yloxy)-N-hydroxyheptanamide (CUDC-101) as a potent multi-acting HDAC, EGFR, and HER2 inhibitor for the treatment of cancer. J. Med. Chem. 53, 2000–2009. https://doi.org/10.1021/jm901453q.

Daina, A., Michielin, O., Zoete, V., 2017. SwissADME: a free web tool to evaluate pharmacokinetics, drug-likeness and medicinal chemistry friendliness of small molecules. Sci. Rep. 7, 42717. https://doi.org/10.1038/srep42717.

Dassault Systèmes BIOVIA, B. D. S. V., version 2019; Dassault Systèmes BIOVIA: San Diego, CA, USA, 2019

Desai, J., Markman, B., Ananda, S., Tebbutt, N.C., Michael, M., Solomon, B.J., McArthur, G.A., Tie, J., Gibbs, P., Ritchie, D., Koldej, R., Herschtal, A., Columbus, R., Ashley, D.M., Lundy, J., Kwan, E.M., Waring, P.M., Tran, B., 2017. A phase I/II trial of combined BRAF and EGFR inhibition in patients (pts) with BRAF V600E mutated (BRAFm) metastatic colorectal (mCRC): the EViCT (Erlotinib and Vemurafenib in Combination Trial) study. J. Clin. Oncol. 35, 3557. https://doi.org/10.1200/JCO.2017.35.15_suppl.3557.

El-Mezayen, N.S., El-Hadidy, W.F., El-Refaie, W.M., Shalaby, T.I., Khattab, M.M., El-Khatib, A.S., 2017. Hepatic stellate cell-targeted imatinib nanomedicine versus conventional imatinib: a novel strategy with potent efficacy in experimental liver fibrosis. J. Control. Release 266, 226–237. https://doi.org/10.1016/j.jconrel.2017.09.035.

El-Sherief, A.M.H., Youssif, G.M.B., Abdelazeem, H.A., Abdel-Aziz, M., Abdel-Rahman, M.H., 2019. Design, Synthesis and Antiproliferative Evaluation of Novel 1,2,4-Triazole/Schiff Base Hybrids with EGFR and B-RAF Inhibitory Activities. Anti-cancer. Agents Med. Chem. https://doi.org/10.2174/1871520619666181224115346.

Franchetti, P., Cappellacci, L., Grifantini, M., Barzi, A., Nocentini, G., Yang, H., O'Connor, A., Jayaram, H.N., Carrell, C., Goldstein, B.M., 1995. Furanfurin and thiophenfurin: two novel tiazofurin analogs. synthesis, structure, antitumor activity, and interactions with inosine monophosphate dehydrogenase. J. Med. Chem. 38, 3829–3837. https://doi.org/10.1021/jm00019a013.

Fu, R., Sun, Y., Sheng, W., Liao, D., 2017. Designing multi-targeted agents: an emerging anti-cancer drug discovery paradigm. Eur. J. Med. Chem. 136, 195–211. https://doi.org/10.1016/j.ejmech.2017.05.016.

Gasteiger, J., Marsili, M., 1980. Iterative partial equalization of orbital electronegativity—a rapid access to atomic charges. Tetrahedron 36, 3219–3228. https://doi.org/10.1016/0040-4020(80)80168-2.

Gomaa, H.A.M., Shaker, M.E., Alzarea, S.I., Hendawy, O.M., Mohamed, F.A.M., Gouda, A.M., Ali, A.T., Morcoss, M.M., Abdelrahman, M.H., Trembleau, L., Youssif, B.G.M., 2022. Optimization and SAR investigation of novel 2,3-dihydropyrazino[1,2-a]indole-1,4-dione derivatives as EGFR and BRAFV600E dual inhibitors with potent antiproliferative and antioxidant activities. Bioorg. Chem. 120,. https://doi.org/10.1016/j.bioorg.2022.105616 105616.

Halgren, T.A., 1999. MMFF VI. MMFF94s option for energy minimization studies. J. Comput. Chem. 20, 720–729. https://doi.org/10.1002/(SICI)1096-987X(199905)20:7<720::AID-JCC7>3.0.CO;2-X.

Hawkins, P.C.D., Skillman, A.G., Warren, G.L., Ellingson, B.A., Stahl, M.T., 2010. Conformer generation with OMEGA: algorithm and validation using high quality structures from the protein databank and cambridge structural database. J. Chem. Inf. Model. 50, 572–584. https://doi.org/10.1021/ci100031x.

Ho, C.-C., Liao, W.-Y., Lin, C.-A., Shih, J.-Y., Yu, C.-J., Chih-Hsin Yang, J., 2017. Acquired BRAF V600E mutation as resistant mechanism after treatment with osimertinib. J. Thorac. Oncol. 12, 567–572. https://doi.org/10.1016/j.jtho.2016.11.2231.

Hu-Lieskovan, S., Mok, S., Homet Moreno, B., Tsoi, J., Robert, L., Goedert, L., Pinheiro, E., Koya, R., Graeber, T., Comin-Anduix, B., Ribas, A., 2015. Improved antitumor activity of immunotherapy with BRAF and MEK inhibitors in BRAFV600E melanoma. Sci. Transl. Med. 7, 279ra41. https://doi.org/10.1126/scitranslmed.aaa4691.

Hyman, D.M., Puzanov, I., Subbiah, V., Faris, J.E., Chau, I., Blay, J.-Y., Wolf, J., Raje, N.S., Diamond, E.L., Hollebecque, A., Gervais, R., Elez-Fernandez, M.E., Italiano, A., Hofheinz, R.-D., Hidalgo, M., Chan, E., Schuler, M., Lasserre, S.F., Makrutzki, M., Sirzen, F., Veronese, M.L., Tabernero, J., Baselga, J., 2015. Vemurafenib in multiple nonmelanoma cancers with BRAF V600 mutations. N. Engl. J. Med. 373, 726–736. https://doi.org/10.1056/NEJMoa1502309.

Ibrahim, M.A.A., Abdelrahman, A.H.M., Atia, M.A.M., Mohamed, T.A., Moustafa, M.F., Hakami, A.R., Khalifa, S.A.M., Alhumaydhi, F.A., Alrumaihi, F., Abidi, S.H., Allemailem, K.S., Efferth, T., Soliman, M.E., Paré, P.W., El-Seedi, H.R., Hegazy, M.-E.-F., 2021a. Blue biotechnology: computational screening of sarcophyton cembranoid diterpenes for SARS-CoV-2 main protease inhibition. Mar. Drugs. https://doi.org/10.3390/md19070391.

Ibrahim, M.A.A., Abdelrahman, A.H.M., Mohamed, T.A., Atia, M. A.M., Al-Hammady, M.A.M., Abdeljawaad, K.A.A., Elkady, E. M., Moustafa, M.F., Alrumaihi, F., Allemailem, K.S., El-Seedi, H. R., Paré, P.W., Efferth, T., Hegazy, M.-E.-F., 2021b. In silico mining of terpenes from red-sea invertebrates for SARS-CoV-2 main protease (Mpro) inhibitors. Molecules 26, 2082. https://doi.org/10.3390/molecules26072082.

Ibrahim, M.A.A., Abdelrahman, A.H.M., Jaragh-Alhadad, L.A., Atia, M.A.M., Alzahrani, O.R., Ahmed, M.N., Moustafa, M.S., Soliman, M.E.S., Shawky, A.M., Paré, P.W., Hegazy, M.-E.-F., Sidhom, P.A., 2022. Exploring toxins for hunting SARS-CoV-2 main protease inhibitors: molecular docking, molecular dynamics, pharmacokinetic properties, and reactome study. Pharmaceuticals. https://doi.org/10.3390/ph15020153.

Jin, K., Yin, H., De Clercq, E., Pannecouque, C., Meng, G., Chen, F., 2018. Discovery of biphenyl-substituted diarylpyrimidines as non-nucleoside reverse transcriptase inhibitors with high potency against wild-type and mutant HIV-1. Eur. J. Med. Chem. 145, 726–734. https://doi.org/10.1016/j.ejmech.2018.01.016.

Li, X., He, Y., Ruiz, C.H., Koenig, M., Cameron, M.D., 2009. Characterization of dasatinib and its structural analogs as CYP3A4 mechanism-based inactivators and the proposed bioactivation pathways. Drug Metab. Dispos. 37, 1242–1250. https://doi.org/10.1124/dmd.108.025932.

LOZYNSKYI Andrii, ZIMENKOVSKY, B., LESYK, R., 2014. Synthesis and Anticancer Activity of New Thiopyrano[2,3-d] thiazoles Based on Cinnamic Acid Amides. Sci. Pharm. https://doi.org/10.3797/scipharm.1408-05

Lv, P.-C., Zhou, C.-F., Chen, J., Liu, P.-G., Wang, K.-R., Mao, W.-J., Li, H.-Q., Yang, Y., Xiong, J., Zhu, H.-L., 2010. Design, synthesis and biological evaluation of thiazolidinone derivatives as potential EGFR and HER-2 kinase inhibitors. Bioorg. Med. Chem. 18, 314–319. https://doi.org/10.1016/j.bmc.2009.10.051.

Madhu Sekhar, M., Nagarjuna, U., Padmavathi, V., Padmaja, A., Reddy, N.V., Vijaya, T., 2018. Synthesis and antimicrobial activity of pyrimidinyl 1,3,4-oxadiazoles, 1,3,4-thiadiazoles and 1,2,4-triazoles. Eur. J. Med. Chem. 145, 1–10. https://doi.org/10.1016/j.ejmech.2017.12.067.

Mahboobi, S., Sellmer, A., Winkler, M., Eichhorn, E., Pongratz, H., Ciossek, T., Baer, T., Maier, T., Beckers, T., 2010. Novel chimeric histone deacetylase inhibitors: a series of lapatinib hybrides as potent inhibitors of epidermal growth factor receptor (EGFR), human epidermal growth factor receptor 2 (HER2), and histone deacetylase activity. J. Med. Chem. 53, 8546–8555. https://doi.org/10.1021/jm100665z.

Martí-Renom, M.A., Stuart, A.C., Fiser, A., Sánchez, R., Melo, F., Šali, A., 2000. Comparative protein structure modeling of genes and genomes. Annu. Rev. Biophys. Biomol. Struct. 29, 291–325. https://doi.org/10.1146/annurev.biophys.29.1.291.

Mohamed, F.A.M., Gomaa, H.A.M., Hendawy, O.M., Ali, A.T., Farghaly, H.S., Gouda, A.M., Abdelazeem, A.H., Abdelrahman, M.H., Trembleau, L., Youssif, B.G.M., 2021. Design, synthesis, and biological evaluation of novel EGFR inhibitors containing 5-chloro-3-hydroxymethyl-indole-2-carboxamide scaffold with apoptotic antiproliferative activity. Bioorg. Chem. 112,. https://doi.org/10.1016/j.bioorg.2021.104960 104960.

Mohassab, A.M., Hassan, H.A., Abdelhamid, D., Gouda, A.M., Youssif, B.G.M., Tateishi, H., Fujita, M., Otsuka, M., Abdel-Aziz, M., 2021. Design and synthesis of novel quinoline/chalcone/1,2,4-triazole hybrids as potent antiproliferative agent targeting EGFR and BRAFV600E kinases. Bioorg. Chem. 106,. https://doi.org/10.1016/j.bioorg.2020.104510 104510.

Morris, G.M., Huey, R., Lindstrom, W., Sanner, M.F., Belew, R.K., Goodsell, D.S., Olson, A.J., 2009. AutoDock4 and AutoDockTools4: automated docking with selective receptor flexibility. J. Comput. Chem. 30, 2785–2791. https://doi.org/10.1002/jcc.21256.

Mostafa, S.M., Aly, A.A., Bräse, S., Nieger, M., Mohamed, A.H., 2022. Facile synthesis of hydrazono bis-4-oxothiazolidines. J. Sulfur Chem. 43, 606–619. https://doi.org/10.1080/17415993.2022.2083454.

Nobuta, T., Hirashima, S., Tada, N., Miura, T., Itoh, A., 2010. ChemInform abstract: facile aerobic photo-oxidative synthesis of phenaryl iodides and bromides from styrenes using I2 or aqueous HBr. Synlett 2010. https://doi.org/10.1055/s-0030-1258022.

Olsson, M.H.M., Søndergaard, C.R., Rostkowski, M., Jensen, J.H., 2011. PROPKA3: consistent treatment of internal and surface residues in empirical pKa predictions. J. Chem. Theory Comput. 7, 525–537. https://doi.org/10.1021/ct100578z.

OMEGA (Version 2.5.1.4). (2013). Santa Fe, NM, USA: OpenEye Scientific Software.

Palmeira, A., Sousa, E., H. Vasconcelos, M., M. Pinto, M., 2012. Three Decades of P-gp Inhibitors: Skimming Through Several Generations and Scaffolds. Curr. Med. Chem 19, 1946-2025. https://doi.org/10.2174/092986712800167392

Pastor, N., Domínguez, I., Vazquez, M.L., Campanella, C., Mateos, S., Cortés, F., 2012. The DNA topoisomerase II catalytic inhibitor

merbarone is genotoxic and induces endoreduplication. Mutat. Res. 738–739, 45–51. https://doi.org/10.1016/j.mrfmmm.2012.07.005.

Pires, D.E.V., Blundell, T.L., Ascher, D.B., 2015. pkCSM: predicting small-molecule pharmacokinetic and toxicity properties using graph-based signatures. J. Med. Chem. 58, 4066–4072. https://doi.org/10.1021/acs.jmedchem.5b00104.

Raghavendra, N.M., Pingili, D., Kadasi, S., Mettu, A., Prasad, S.V.U. M., 2018. Dual or multi-targeting inhibitors: the next generation anti-cancer agents. Eur. J. Med. Chem. 143, 1277–1300. https://doi.org/10.1016/j.ejmech.2017.10.021.

Rizk, S.A., El-Naggar, A.M., El-Badawy, A.A., 2018. Synthesis, spectroscopic characterization and computational chemical study of 5-cyano-2-thiouracil derivatives as potential antimicrobial agents. J. Mol. Struct. 1155, 720–733. https://doi.org/10.1016/j.molstruc.2017.11.066.

Saleeb, M., Sundin, C., Aglar, Ö., Pinto, A.F., Ebrahimi, M., Forsberg, Å., Schüler, H., Elofsson, M., 2018. Structure–activity relationships for inhibitors of Pseudomonas aeruginosa exoenzyme S ADP-ribosyltransferase activity. Eur. J. Med. Chem. 143, 568–576. https://doi.org/10.1016/j.ejmech.2017.11.036.

Santi, D.V., McHenry, C.S., Sommer, H., 1974. Mechanism of interaction of thymidylate synthetase with 5-fluorodeoxyuridylate. Biochemistry 13, 471–481. https://doi.org/10.1021/bi00700a012.

Shaker, M.E., Ghani, A., Shiha, G.E., Ibrahim, T.M., Mehal, W.Z., 2013. Nilotinib induces apoptosis and autophagic cell death of activated hepatic stellate cells via inhibition of histone deacetylases. Biochim. Biophys. Acta - Mol. Cell Res. 1833, 1992–2003. https://doi.org/10.1016/j.bbamcr.2013.02.033.

Sharma, P.C., Jain, A., Yar, M.S., Pahwa, R., Singh, J., Chanalia, P., 2017. Novel fluoroquinolone derivatives bearing N-thiomide linkage with 6-substituted-2-aminobenzothiazoles: synthesis and antibacterial evaluation. Arab. J. Chem. 10, S568–S575. https://doi.org/10.1016/j.arabjc.2012.11.002.

Stamos, J., Sliwkowski, M.X., Eigenbrot, C., 2002. Structure of the epidermal growth factor receptor kinase domain alone and in complex with a 4-anilinoquinazoline inhibitor. J. Biol. Chem. 277, 46265–46272. https://doi.org/10.1074/jbc.m207135200.

Stanković, T., Dinić, J., Podolski-Renić, A., Musso, L., Burić, S.S., Dallavalle, S., Pešić, M., 2019. Dual inhibitors as a new challenge for cancer multidrug resistance treatment. Curr. Med. Chem. https://doi.org/10.2174/0929867325666180607094856.

SZYBKI 1.9.0.3, OpenEye Scientific Software: Santa Fe, NM, USA, 2016.

Tang, B., Tang, P., He, J., Yang, H., Li, H., 2018. Characterization of the binding of a novel antitumor drug ibrutinib with human serum albumin: insights from spectroscopic, calorimetric and docking studies. J. Photochem. Photobiol. B Biol. 184, 18–26. https://doi.org/10.1016/j.jphotobiol.2018.05.008.

Trott, O., Olson, A.J., 2010. AutoDock Vina: Improving the speed and accuracy of docking with a new scoring function, efficient optimization, and multithreading. J. Comput. Chem. 31, 455–461. https://doi.org/10.1002/jcc.21334.

Zha, G.-F., Qin, H.-L., Youssif, B.G.M., Amjad, M.W., Raja, M.A. G., Abdelazeem, A.H., Bukhari, S.N.A., 2017. Discovery of potential anti-cancer multi-targeted ligustrazine based cyclohexanone and oxime analogs overcoming the cancer multidrug resistance. Eur. J. Med. Chem. 135, 34–48. https://doi.org/10.1016/j.ejmech.2017.04.025.

Zheng, W., Zhao, Y., Luo, Q., Zhang, Y., Wu, K., Wang, F., 2017. Multi-targeted anticancer agents. Curr. Top. Med. Chem. 17, 3084–3098. https://doi.org/10.2174/1568026617666170707124126.